PHYSICAL REVIEW B VOLUME 25, NUMBER 5 1 MARCH 1982

Nonlinear renormalization-group analysis of the thermal conductivity of ^{4}He for $T \geq T_\lambda$

Guenter Ahlers
Bell Laboratories, Murray Hill, New Jersey 07974
and University of California, Santa Barbara, California 93106

P. C. Hohenberg and A. Kornblit
Bell Laboratories, Murray Hill, New Jersey 07974

(Received 30 April 1981; revised manuscript received 23 November 1981)

The thermal conductivity of ^{4}He above the superfluid transition is analyzed using nonlinear renormalization-group recursion relations. Experimental data are presented over a wide temperature range and for various pressures. The dynamic coupling constant far from T_λ is a small parameter which leads to the possibility of a rigorous test of the theory in a region where perturbation theory is valid. Closer to T_λ the system crosses over to the scaling regime at a reduced temperature $t_c \approx 10^{-3}$, whose smallness results from the weak dynamic coupling far from T_λ. Detailed tests of the theory are presented over the whole temperature range above T_λ, and consistency is found with the asymmetric-spin model (F) of Halperin, Hohenberg, and Siggia if corrections are introduced to compensate for truncation errors in the perturbation expansion. The symmetric model (E), on the other hand, shows significant deviations from the data even in regions where perturbation theory should hold. The analysis implies a value $d^* \lesssim 2.6$ for the dimensionality below which dynamic scaling breaks down. This value is lower than earlier estimates ($d^* \approx 3$).

I. INTRODUCTION

The dynamic-scaling prediction[1] for the critical divergence of the thermal conductivity λ of ^{4}He as T approaches T_λ, was dramatically confirmed by macroscopic measurements over many decades in reduced temperature.[2,3] Subsequent refinements in the experiments,[4] however, as well as other measurements in thin cells,[5–7] found deviations from the theoretical prediction. Specifically, the experiments revealed (i) a strong dependence of λ on the cell height h even for h much larger than the correlation length ξ, (ii) an effective exponent for λ which was slightly larger than the dynamic-scaling prediction, and (iii) a critical region for λ ($t < t_c \approx 10^{-3}$) which was much narrower than the critical region for the statics ($t \lesssim 10^{-1}$). These results call for a quantitative theoretical explanation.

The dynamic-scaling theory[1,8,9] originally proposed on purely phenomenological grounds, was confirmed by renormalization-group calculations[10–12] which relied on the continuity of an expansion in $\epsilon = 4 - d$, where d is the dimensionality of space. These calculations obtained a few terms in the ϵ expansion, but did not yield reliable values for the universal amplitude of the diverging thermal conductivity in three dimensions. In 1977 DeDominicis and Peliti[13] pointed out that the continuity argument may break down before one reaches three dimensions, due to the instability of the dynamic-scaling fixed point, to another fixed point, which they termed "weak scaling." In that regime the characteristic frequency ω_ψ for the order parameter vanishes with a larger scaling exponent than the entropy frequency ω_m; i.e., their ratio $w \approx \omega_\psi/\omega_m$ scales to zero at T_λ (if dynamic scaling holds w goes to a positive limit w^*). Various theoretical estimates[14–18] of the critical dimensionality d^* for breakdown of dynamic scaling all gave $d^* \approx 3 \pm 0.2$.

A number of authors realized at that point that the weak-scaling instability would be accompanied by anomalous slow transients,[12,13,16] and the first quantitative theory for λ was put forward by Ferrell and Bhattacharjee[19] who emphasized the following points: (i) The small value of w^* implies a large amplitude for the corresponding slow transient near the fixed point. (ii) The smallness of the dynamic critical region requires a quantitative explanation. (iii) There exists a high-temperature regime[20,21] where the small departures of λ from its constant background value can be calculated using a perturbation expansion in $\kappa^{-1} = t^{-\nu}$. As shown in detail below, however, the quantitative aspects of their analysis are not accurate, since the theory was applied outside of its domain of validity.

In a related paper, Hohenberg, Halperin, and Nelson[18] pointed out the difficulty of detecting the weak-scaling instability by analyzing thermal conductivity data. These authors proposed a "quadratic approximation" in which the slow transient associated with the instability is taken into account exactly to first order in the small parameter w^*. In order to test this representation they proposed[22] an analysis based

on a numerical integration of the truncated renormalization-group recursion relations, treating the nonuniversal initial values as adjustable parameters. The present work[23] is the result of this suggestion.

Independently of Ref. 18, Dohm and Folk[24,25] introduced a similar nonlinear analysis of the data, confining themselves to the symmetric model of Halperin, Hohenberg, and Siggia[11] (model E). These authors were, in fact, the first to carry out such an analysis, and they reported excellent agreement with experiment, with d^* determined by the data to be very close to 3.

The present paper takes up the nonlinear analysis from a more general and more precise point of view; we consider both a broader class of theoretical models and more extensive experimental data than in Refs. 24 and 25 (some of the data we analyze[26] were previously unpublished). Our conclusion is that previous claims[19,24,25] of a quantitative confirmation of the theory are not fully justified. Indeed, uncertainties in both theory and experiment for reduced temperatures $t \lesssim 10^{-4}$ prevent an unambiguous determination of d^*, or of the asymptotic critical behavior in three dimensions. Nevertheless, the theory can be meaningfully tested for $t \gtrsim 10^{-4}$, due to an important effect which had not been properly appreciated in the previous literature. This is the existence of a small parameter[23] associated with the weakness of the *bare* dynamic coupling constant (far from T_λ) $f_b \approx 0.02$. If f_b were zero, the thermal conductivity would obey the Van Hove theory[12] and remain constant up to T_λ. For any nonzero f_b, the renormalized coupling constant $f(t)$ evolves as a function of temperature, approaching the fixed-point value $f^* = O(1)$ at T_λ, independent of the initial value f_b. The passage from weak coupling ($f \ll 1$) to critical behavior ($f \approx 1$) occurs at a characteristic crossover[27] temperature t_c which becomes vanishingly small in the limit $f_b \to 0$. Thus, the whole weak-coupling range as well as the crossover region offer the possibility of nontrivial comparison between experiment and theory, using perturbation theory.

We find that the previously used[18,25] symmetric-spin model[11] (E) shows perceptible deviations from the data in the range $10^{-3} < t < 10^{-2}$ where perturbation theory should hold. The asymmetric model[11] (F), which takes the specific-heat singularity into account consistently, fits experiment satisfactorily in this range. When extended to the range $t < 10^{-3}$ the theory does not agree with experiment, but the discrepancy can be attributed to truncation errors in the perturbation expansion[11,13,17] which cannot be neglected when $f \approx 1$. As a way of correcting for these errors, we have introduced[23] a phenomenological three-loop term in the equations, and treated its coefficient as an additional adjustable parameter. The ensuing fit is excellent for model F over the whole temperture range, but it remains unsatisfactory for model E. Another way to analyze the data is to use the high-temperature expansion of Ferrell and Bhattacharjee.[20,21] If proper account is taken of *regular* transients, one can use the data for $t > 10^{-2}$ to determine initial values at $t = 10^{-2}$, and then predict the behavior for $t < 10^{-2}$ *with essentially no adjustable parameters.* This procedure yields excellent agreement until $t \approx 10^{-3}$, where truncation errors become important, as mentioned above.

Having fixed the parameters of the theory from an analysis above T_λ, we may follow the procedure of Dohm and Folk[24,28] to predict the second-sound damping[29–31] below T_λ, without further adjustable parameters (a similar procedure was subsequently used by Ferrell and Bhattacharjee[32] in the weak-coupling regime below T_λ). We find some uncertainty in the predictions due to uncertainties in the *static* critical behavior. For one natural choice of static parameters, however, we obtain excellent agreement with experiment at vapor pressure and reasonable consistency with available data at higher pressure.

Section II presents the experimental data of Ref. 4 at several pressures, as well as new data at vapor pressure,[26] and compares these with the measurements of Archibald *et al.*[5,6] and Weaver[7] on thin cells. The cell-size dependence of the critical thermal conductivity in the latter experiments implies that the measurements of Ref. 4 may not correspond quantitatively to the bulk limit (the physical origin of this dependence is not known at present). We shall only analyze the data of Ahlers[4] (cell D) and the new data[26] (cell A) because of lesser precision in the other measurements, and because we have no way of taking the size dependence into account.

Section III reviews the theoretical situation, with special emphasis on the dependence of the quantitative results on the parameters of the theory. The analysis of the data is carried out in Sec. IV, first in terms of power laws, to show how misleading such analyses can be, and then in terms of nonlinear recursion relations. The different models are treated successively, and the high-temperature expansion tested quantitatively. Section V contains a discussion and critique of previous work on this subject, and concludes with a summary of the present results, as well as a program for experimental and theorical improvements. Details of the high-temperature expansion are described in the Appendixes.

II. EXPERIMENTAL DATA

A. Thermal conductivity measurements

Simultaneous with the development in the late 1960's of the dynamic scaling theory[1,9–11] of transport properties near the λ point and the prediction[1] of a divergent thermal conductivity in He I, experimental evidence for a strong singularity in λ was presented

by Kerrisk and Keller.[33] Very soon thereafter, rather detailed measurements became available from two separate laboratories.[2,3,5,6] These results to a large extent confirmed the predictions of the theory at a semiquantitative level, but they also raised some important, as yet unresolved, questions. In particular, the measurements by Archibald *et al.*[5,6] were made in thermal conductivity cells whose spacings h were small, but macroscopic in comparison to the correlation length. Surprisingly, they showed a strong size dependence near T_λ, with λ diverging more rapidly for smaller h, corresponding to a larger effective exponent than the theory had predicted. The measurements by Ahlers[2] were made in a cell of very large spacing ($h=1$ cm), and agreed within their resolution with the theory. To illustrate the size dependence, the effective exponents derived from various measurements are shown as a function of h in Fig. 1. It is seen that for $h=0.003$ cm the exponent is twice as large as the theory predicts (dashed line), whereas for large h the agreement is much better. The correlation length in the experimental temperature range is less than 10^{-4} cm, and thus the strong size dependence is not readily understood from a theoretical viewpoint. A possible mechanism for understanding the data is nonlinear heat conduction, which could be associated with macroscopic lengths in the critical region.[34] Of course, this interpretation implies that the measured λ was not the zero-current limit of the conductivity, a point which can be tested by further experiments.

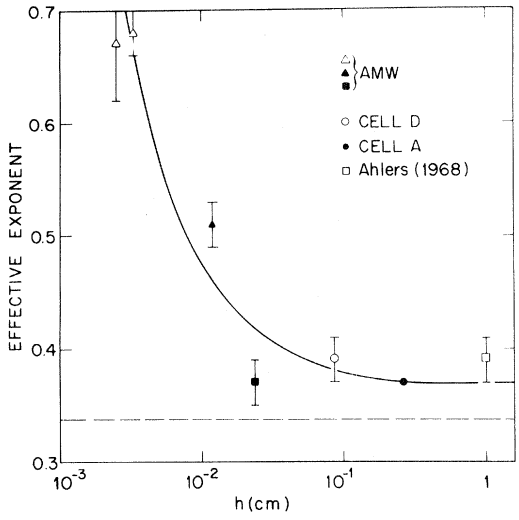

FIG. 1. Effective exponent of the thermal conductivity plotted as a function of cell height h on a logarithmic scale. The points marked AMW are from Archibald *et al.* (Ref. 6) and the open square is from Ref. 2. The dashed line is the theoretical asympotic value $\frac{1}{2}\nu=0.338$. The error bars correspond to the error estimates of the respective authors.

Although the effective exponents in Fig. 1 are not very precise, the data suggest that true bulk behavior at a highly quantitative level may not be reached until $h \gtrsim 0.3$ cm. This is illustrated by the solid line in the figure, which has no significance other than being a smooth representation of the data. The measurements in the 1-cm cell can surely be regarded as being in the bulk limit, but experiments in such a large cell are difficult because the thermal relaxation times for the establishment of steady-state gradients become as large as an hour or so. Because of limits on the long-term thermal stability of the apparatus, the resulting scatter in the data of Ref. 2 was thus as large as a few percent.

Much more precise data at several pressures were obtained in 1970 in a cell of 0.09-cm spacing[4] (this cell will be referred to as cell D). These data had a scatter of only about 0.1% except at the smallest values of reduced temperature t, where temperature resolution of about 10^{-7} K was a limiting factor. Inspection of Fig. 1, however, suggests that these data may also not be entirely in the bulk limit and may for that reason differ slightly from ideal behavior. In addition, the construction of this cell[35] made it impossible to obtain accurate measurements of the contribution from the cell walls to the total conduction, because the effective thermal length of the walls changed when the cell was filled with helium. The wall conduction thus had to be estimated from the known thermal conductivity of stainless steel and the cross-sectional area of the walls. This estimate yielded liquid-^{4}He conductivities at high temperatures and conductivities for ^{4}He gas[35] which agreed well with the data of Kerrisk and Keller.[33] At these temperatures (say 2.2 K) and when the cell was filled with liquid ^{4}He at vapor pressure, the wall contribution to the total conduction was about 20%. Close to T_λ the relative contribution from the walls becomes much smaller because of the divergent conductivity of the liquid. However, close to T_λ, the boundary (Kapitza) resistance between the copper plates and the liquid and any series resistance in the plates become appreciable because they are essentially independent of T, whereas the thermal resistance of the liquid vanishes at T_λ. The largest correction for the boundary and series resistances, say at $t=5\times10^{-6}$, amounted to about 13% of the total resistance. It is difficult to estimate the uncertainties associated with the wall conduction and boundary resistance, but systematic errors of a few percent which may vary with t might be expected for λ as determined in this cell. The measurements at pressures greater than vapor pressure were made along isochores, and the values of λ and t were corrected to values along isobars using a procedure similar to the one employed by Greywall and Ahlers for second-sound velocity measurements.[36]

A final set of measurements, previously unpublished, was obtained in 1977 by Ahlers and Behr-

inger[26] in a cell of spacing $h=0.26$ cm (to be referred to a cell A). This spacing yielded thermal relaxation times of order 5 min, and permitted high-precision measurements. The construction of cell A is described in detail by Behringer and Ahlers.[37] Special provisions were made to permit the experimental determination of the wall conduction, and the measured values agreed well with the thermal conductivity of stainless steel. For the spacing of this cell, the boundary resistance correction remained small even at the smallest values of t. We therefore regard the measurements in this cell as somewhat more reliable than the data obtained with cell D. For large t, the data obtained with cell A agree well with the results of Kerrisk and Keller.[33] On the basis of Fig. 1, the spacing of this cell is probably large enough for the measurements to correspond to the bulk limit, and to warrant a very detailed comparison with theoretical predictions. In order to establish this point more clearly, however, and also because of the intrinsic interest of the unexpectedly large size effect suggested by the previous data,[5,6] more quantitative measurements in the range $h \lesssim 0.3$ cm are highly desirable, and planned for the future. Accurate measurements at small h are difficult and have to deal with a number of experimental problems involving precise measurements of h, accurate correction for wall conduction, and the determination of the boundary resistance which becomes more important as h decreases. For the present, we shall compare the results of the theory with data from cells A and D. We will keep in mind, however, that the experimental situation is not as definitive as one would like for comparison with the very detailed theoretical predictions which are now available.

The measured values of reduced temperature t and thermal conductivity λ for cell D at four pressures, and for cell A at saturated vapor pressure are available elsewhere.[38]

B. Determintaion of $\hat{R}_\lambda$

For comparison with the theoretical predictions[18,19,25] the thermal conductivity λ may be reexpressed in terms of the effective amplitude[11,39]

$$\hat{R}_\lambda(t)=\lambda/g_b(\xi C_P)^{1/2} , \tag{2.1}$$

where

$$g_b=\sigma_\lambda k_B T_\lambda/\hbar , \tag{2.2}$$

$\sigma_\lambda=S_\lambda/R$ is the (dimensionless) entropy at T_λ, and R is the gas constant. In Eq. (2.1) C_P is the constant-pressure specific heat per unit volume and

$$\xi=\xi_0 t^{-\nu} \tag{2.3}$$

is the correlation length, where

$$\xi_0=1.41\ \text{Å} \tag{2.4}$$

at all pressures,[40] the exponent ν is given by[41]

$$\nu=0.675 , \tag{2.5}$$

and

$$t=[T-T_\lambda(P)]/T_\lambda(P) \tag{2.6}$$

is the reduced temperature. In order to obtain g_b, Eq. (2.2), we have used values of σ_λ evaluated in Ref. 42, and shown in Table I. The specific heat can

TABLE I. Thermodynamic parameters. (References are given in Sec. II A.)

P (bars)	T_λ (K)	V_λ (cm^3/mole)	S_λ (J/mole K)	σ_λ	g_b (10^{11} sec^{-1})
0.05	2.1720	27.38	6.24	0.750	2.134
6.85	2.1009	25.41	5.71	0.687	1.889
14.73	2.0024	23.99	5.25	0.631	1.653
22.30	1.8930	22.99	4.87	0.586	1.452
29.00	1.784	22.29	4.54	0.546	1.275

P (bars)	A (J/mole K)	B (J/mole K)	D	E (J/mole K)	α
0.05	6.797	257.77	−0.022	95.73	−0.025
6.85	6.607	237.2	−0.103	0	−0.026
14.73	6.498	229.8	−0.180	0	−0.026
22.30	6.776	235.5	−0.275	0	−0.026

be written

$$C_P = (A/\alpha)t^{-\alpha}(1 + Dt^{0.5}) + B + Et \quad . \tag{2.7}$$

At vapor pressure, a fit of specific heat data for $t \lesssim 0.05$ gave the coefficients in Table I.[42] At higher pressures, direct measurements of C_P have not been made. Instead, C_P has been derived from C_V and other thermodynamic information.[43] Therefore, we consider it more reliable to use C_P values derived from measurements[44] of the thermal expanison coefficient β_p, using the relation[42]

$$C_P = T\left(\frac{\partial S}{\partial T}\right)_\lambda + TV\left(\frac{\partial P}{\partial T}\right)_\lambda \beta_p + O(t) + O(t^{1-\alpha}) \quad , \tag{2.8}$$

and neglecting terms of higher order in t. We used $(\partial P/\partial T)_\lambda$ as determined by Kierstead,[45] and $(\partial S/\partial T)_\lambda$ from Ref. 42. For β_p we used Eqs. (5.2)–(5.4) and Table IV of Ref. 44. The measured values of T_λ and of V_λ,[45] as well as the coefficients of Eq. (2.7) are also given in Table I, and should yield reliable C_P values for $t < 3 \times 10^{-3}$.

In Fig. 2 we show the values of $\hat{R}_\lambda$ which were derived from thermal conductivity measurements at several pressures in cell D. The data at vapor pressure are compared with the measurements of Archibald *et al.*[5,6] and Weaver[7] for several cell spacings h in Fig. 3. The dependence of $\hat{R}_\lambda$, and thus of λ, on the cell spacing h is evident in this figure. The

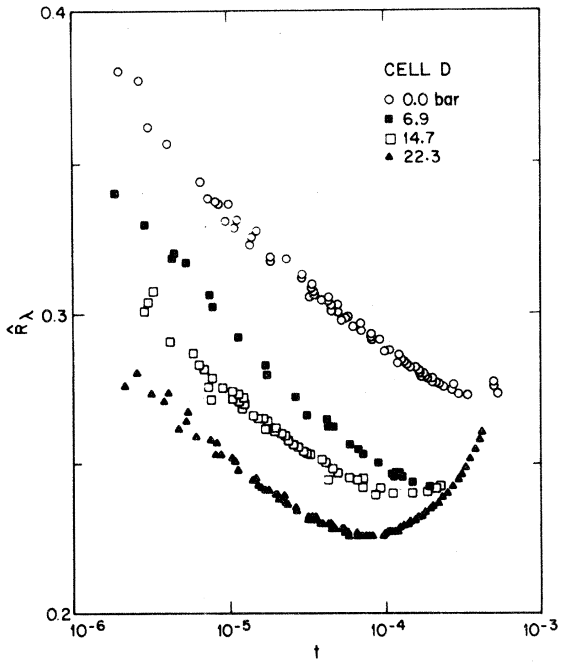

FIG. 2. Effective amplitude $\hat{R}_\lambda$ [Eq. (2.1)] of the thermal conductivity in cell D (Ref. 4) for different pressures, as a function of reduced temperature.

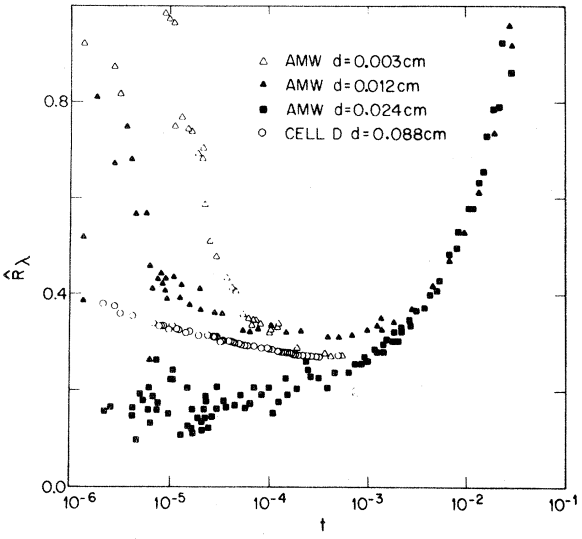

FIG. 3. Effective amplitude $\hat{R}_\lambda$ [Eq. (2.1)] vs reduced temperature for the data for Archibald *et al.* (Ref. 6) and for cell D. The symbols are as in Fig. 1.

results for cells A and D at vapor pressure will be compared in Figs. 5 and 18 below.

In Sec. IV we shall carry out least-squares fits of the data to various theoretical expressions. We used the data in Ref. 38, except that for cell A and $t < 0.003$ only one-third of the data points (i.e., points 1, 4, 7, . . .) were included in the fits (for larger t, all points were used). In these fits we used weights which are equal to the inverse of the square of the probable error for each data point. For an *a priori* estimate of the probable errors in λ we used $10^{-3}\lambda$ when $t > 5 \times 10^{-5}$, because in that temperature range the precision of the data generally was about 0.1%. For smaller t, temperature resolution usually limited the precision of the data, and we used $(5 \times 10^{-8}/t)\lambda$ for the error estimate. In principle, it would be better to use the actual values of the temperature differences employed in the measurements, for the error estimates, but for small t these differences were not much smaller than $T_\lambda t$.[23]

C. High-temperature expansion of λ

It was suggested by Ferrell and Bhattacharjee[20,21] that there exists a high-temperature expansion of λ in the form

$$\lambda = \lambda_H = \lambda_\infty(1 + \lambda_1 t^{-\nu} + \lambda_2 t^{-2\nu} + \cdots) \quad . \tag{2.9}$$

We derive this expansion below for our theoretical models, and discuss the range of validity of Eq. (2.9) in detail. Here, we would like to examine this relation empirically by plotting λ as a function of $t^{-\nu}$ with $\nu = 0.675$. This is done in Fig. 4 for the cell-D data at various pressures, and in Fig. 5 for the cell-A and

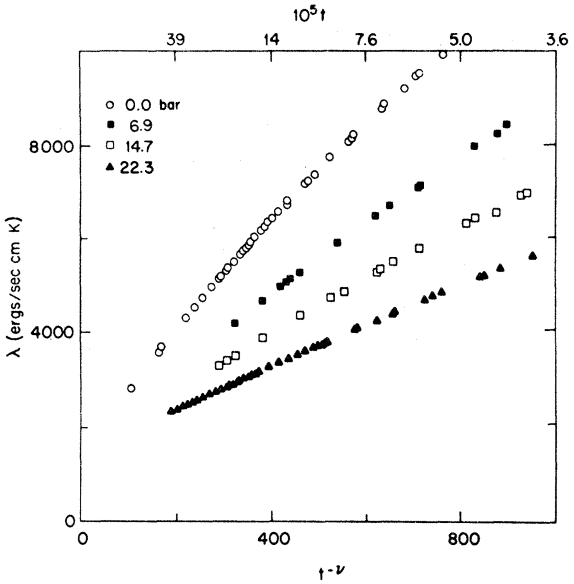

FIG. 4. Portion of the data of Fig. 2 plotted as λ vs $\kappa^{-1}=t^{-\nu}$, as suggested in Ref. 20. The top scale gives the reduced temperature.

cell-D data at vapor pressure. In each case, the data tend to approach a straight line at small $t^{-\nu}$, consistent with Eq. (2.9) and with the observations by Ferrell and Bhattacharjee at 22.3 bars (Ref. 20) and at vapor pressure[32] for cell D. We note that the cell-A and cell-D data at vapor pressure (Fig. 5) extrapolate to very nearly the same value λ_∞ at $t^{-\nu}=0$ ($t\to\infty$), consistent with the statement, made above, that both sets of data at high t agree with the measurements by Kerrisk and Keller.[33] We have performed a least-squares fit of the data in Figs. 4 and 5 to Eq. (2.9) and obtained the parameters in Table II. For this purpose, we used data over the range $t\gtrsim 4\times10^{-5}$, $3000\lesssim\lambda\lesssim10^4$ erg/sec cm K roughly consistent with the range used by Ferrell and Bhattacharjee in their analysis.[20] The values of λ_∞ at vapor pressure for cells A and D differ by only 2%, but they are considerably larger than our estimate to be given in Sec. IV C, below, of the actual high-temperature limit of the expansion, Eq. (2.9). As explained there, this difference arises because the data used in the fit are not at sufficiently high values of t for the expansion to be valid. The actual range of validity turns out to be $t^{-\nu}<\kappa_c^{-1}$, with $\kappa_c^{-1}=125$ shown in Fig. 5.

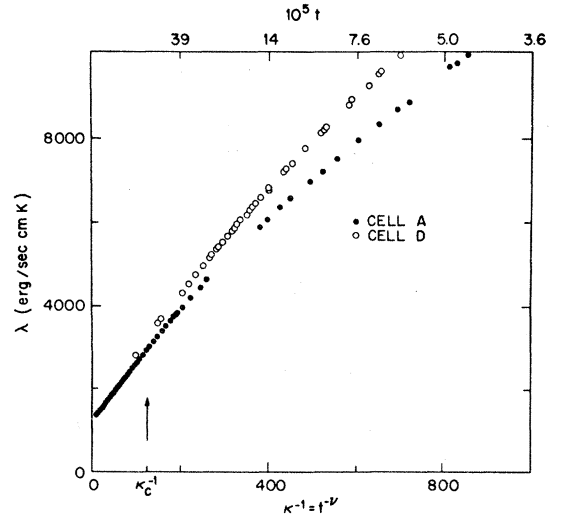

FIG. 5. Comparison of the data at vapor pressure in cell A (Ref. 27) and cell D (Ref. 4), plotted as in Fig. 4. The high-temperature expansion of Sec. III C is only accurate for $t^{-\nu}\lesssim\kappa_c^{-1}=\lambda_1^{-1}=125$ [see Eq. (3.41) below].

TABLE II. Fit of thermal conductivity to Eq. (29) in the range $\kappa^{-1}=t^{-\nu}<1000$ for cell A, and cell D at four different pressures.

Fit	Cell	λ_∞ (erg/sec cm K)	$10^2\lambda_1$	$10^6\lambda_2$
1	A	1472	0.808	−2.07
2	D 0.0	1441	0.971	−2.54
3	D 6.9	1472	0.607	−0.863
4	D 14.7	1390	0.509	−0.813
5	D 22.3	1445	0.337	−0.298

D. Generation of "data" for cell D at high t

The measurements for cell D unfortunately were made only for $t\lesssim10^{-3}$. For comparison with the theoretical models, it is useful to have data at larger t. We therefore generated cell-D data at vapor pressure from the measurements in cell A for $t\gtrsim10^{-3}$, using the formula

$$\lambda(\text{cell } D)=\lambda(\text{cell } A)+[\lambda_H(\text{cell } D)-\lambda_H(\text{cell } A)]\ , \tag{2.10}$$

with λ_H given by Eq. (2.9) and calculated from the coefficients in Table II. Since only the small difference $\lambda_H(\text{cell } D)-\lambda_H(\text{cell } A)$ is extracted from the expansion, we expect this procedure to yield a good approximation to the actual conductivity of cell D. In any event, we have carried out all of our analyses below for both cells A and D and our basic conclusions do not depend on which set of data is used.

E. High-temperature data

In the range $t>0.05$, there are not thermal conductivity data for either cell A or D. We shall, there-

TABLE III. High-temperature data a vapor pressure. (References are given in Sec. II E.)

T (K)	V (cm^3/mole)	C_P (J/mole K)	σ	$g_b(T)$ (10^{11} sec^{-1})	λ (erg/cm sec K)
2.3	27.48	10.59	0.838	2.523	1419
2.4	27.56	9.56	0.891	2.800	1462
2.6	27.77	9.16	0.973	3.312	1550
2.8	28.02	9.49	1.055	3.867	1630
3.0	28.36	10.17	1.136	4.462	1700
3.2	28.76	11.09	1.218	5.103	1763
3.4	29.25	12.39	1.305	5.809	1816
3.6	29.81	13.79	1.430	6.740	1861
3.8	30.56	15.52	1.473	7.328	1903
4.0	31.18	17.65	1.570	8.222	1942
4.2	32.00	20.53	1.666	9.161	1974

fore, use the measurements by Kerrisk and Keller,[33] which agree well with cell A near $t=0.05$. These authors fitted their results to an empirical equation which gives $\lambda(P,T)$. The extrapolation of this equation to vapor pressure seems less reliable than a graphical extrapolation of the measurement on a particular isotherm to vapor pressure. Therefore, we used the latter procedure, with measured values of λ reported by Kerrisk.[46] The results are given in Table III.

When needed, we also used specific-heat measurements at large t by Hill and Lounasmaa.[47] These data are for the specific heat at saturated vapor pressure C_s. Whereas the difference between C_P and C_s is negligible below 2.2 K, it becomes appreciable at higher T. Values of C_P were therefore calculated[48] from C_s and other available thermodynamic information and are listed in Table III, along with values of the molar volume V, the dimensionless entropy σ, and a finite-temperature generalization of the coupling constant g_b of Eq. (2.2), to be discussed below.

III. THEORY

A. Definitions and review of earlier work

Our starting point[11] is a dynamical model involving the complex superfluid order parameter $\psi(x,t)$, and the entropy variable $m(x,t)$ (a real field), satisfying the equations of motion[49]

$$\frac{\partial\psi}{\partial t}=-2\Gamma_b\frac{\delta F_b}{\delta\psi^*}-ig_b\psi\frac{\delta F_b}{\delta m}+\theta\ , \tag{3.1a}$$

$$\frac{\partial m}{\partial t}=\lambda_b\nabla^2\frac{\delta F_b}{\delta m}+2g_b\,\mathrm{Im}\left[\psi^*\frac{\delta F_b}{\delta\psi^*}\right]+\zeta\ , \tag{3.1b}$$

where

$$F_b=\int d^dx\left(\tfrac{1}{2}\tilde{r}_b|\psi|^2+\tfrac{1}{2}|\nabla\psi|^2+\tilde{u}_b|\psi|^4+\tfrac{1}{2}C_{Pb}^{-1}m^2+\gamma_b m|\psi|^2\right)\ , \tag{3.1c}$$

d is the dimensionality of space, λ_b, g_b, $\tilde{r}_b$, $\tilde{u}_b$, C_{Pb}, and γ_b are real constants, while Γ_b is complex. The noise functions θ and ζ are Gaussian and satisfy the usual fluctuation-dissipation relations; the fields $\psi(x,t)$ and $m(x,t)$ are assumed to have spatial Fourier components less than some cutoff $\Lambda_c=\xi_0^{-1}$. When the renormalization-group procedure is applied to (3.1) one obtains the usual[50] $n=2$ result for the *static* properties, and one can express the dynamical behavior in terms of two renormalized frequency ratios[51]

$$w(l)=\frac{\omega_\psi(l)}{\omega_m(l)}=\frac{\Gamma(l)C_P(l)}{\lambda(l)} \tag{3.2}$$

and

$$f(l)=\frac{K_d\omega_c^2(l)}{\omega_\psi(l)\omega_m(l)}=\frac{K_d g_b^2\Lambda_c^{-\epsilon}}{\lambda(l)\,\mathrm{Re}\Gamma(l)\kappa^\epsilon}\ , \tag{3.3}$$

and two static coupling constants

$$u(l)=\tilde{u}(l)-\tfrac{1}{2}\gamma^2(l)C_P(l) \tag{3.4}$$

and

$$v(l)=K_d\gamma^2(l)C_P(l)\Lambda_c^{-\epsilon}\ . \tag{3.5}$$

In Eqs. (3.2)–(3.5) the scale parameter l is defined by the relation

$$\kappa=t_0^\nu e^{-l}\ , \tag{3.6}$$

where t_0 is an arbitrary scale, and κ is the *dimensionless* inverse correlation length

$$\kappa=t^\nu\ . \tag{3.7}$$

The constant K_d is given by

$$K_d^{-1}=2^{d-1}\pi^{d/2}\Gamma(\tfrac{1}{2}d) \ , \tag{3.8}$$

where in Eq. (3.8) (and only there) $\Gamma(a)$ is the gamma function. The quantites $\lambda(l)$, $\Gamma(l)$, $C_P(l)$, $\gamma(l)$, and $\tilde{u}(l)$ are suitably renormalized versions of the corresponding bare parameters, whose precise definitions depend on the particular renormalization procedure employed.

The parameters $f(l)$ and

$$w(l)=w'(l)+iw''(l) \tag{3.9}$$

satisfy nonlinear recursion relations[13]

$$\frac{df}{dl}=-\beta_f(f,w,v,u) \ , \tag{3.10}$$

$$\frac{dw}{dl}=-\beta_w(f,w,v,u) \ , \tag{3.11}$$

where the β functions are only known as power series in the dynamic coupling constant f and the static couplings u and v, whose coefficients are obtained to all orders in the ratio w. In the present work we shall assume that u has reached its fixed-point value u^*, i.e., that κ is given by a pure power law (3.7). The coupling constant v, Eq. (3.5), is related to the specific heat by[11]

$$v=\frac{\alpha_e}{4\nu}\equiv\frac{d\ln C_P}{4dl}=-\frac{d\ln C_P}{4d\ln\kappa} \ , \tag{3.12}$$

and will be taken from the measured temperature dependence of C_P, except at high temperatures when (3.12) ceases to be valid (see Appendix A).

Given the functions $f(l)$ and $w(l)$, the thermal conductivity is given by[11,18]

$$\lambda=\hat{R}_\lambda g_b C_P^{1/2}\xi_0^{\epsilon/2}\kappa^{-\epsilon/2} \ , \tag{3.13}$$

with

$$\epsilon=4-d \tag{3.14}$$

and

$$\hat{R}_\lambda(t)=K_d^{1/2}[f(l)w'(l)]^{-1/2}[1+P(l)] \ . \tag{3.15}$$

Equation (3.13) generalizes Eq. (2.1) to arbitrary d. The factor $P(l)$ has a perturbation expansion in f, v, and u, analogous to the one for the β functions.

We shall use the form of perturbation theory obtained by De Dominicis and Peliti,[13] and Dohm,[17] which to second order in f reads[18,51]

$$\beta_f=-f\left[\epsilon+A_1(w')f+A_2(w')f^2+\eta^A-\frac{1}{w'}\mathrm{Re}(w\tilde{h})\right] \ , \tag{3.16}$$

$$\beta_w=-w[B_1(w')f+B_2(w')f^2-\eta^A+4v-\tilde{h}] \ , \tag{3.17}$$

$$\tilde{h}=\frac{1}{1+w}\left[f\frac{w'}{w}-4vw-4i(fvw')^{1/2}\right]-\frac{f}{1+w'} \ , \tag{3.18}$$

$$A_1(w)=\left[\frac{1}{2}+\frac{1}{1+w}\right] \ , \tag{3.19}$$

$$A_2(w)=L(w)+G(w) \ , \tag{3.20}$$

$$B_1(w)=-\left[\frac{1}{2}-\frac{1}{1+w}\right] \ , \tag{3.21}$$

$$B_2(w)=L(w)-G(w) \ , \tag{3.22}$$

$$L(w)=\frac{1}{4(1+w)}\left[w^2(2+w)\ln\left[\frac{(1+w)^2}{w(2+w)}\right]-w-\tfrac{1}{2}\right] \ , \tag{3.23}$$

$$G(w)=\frac{1}{8(1+w)^3}\left[4(1+2w)\ln\left[\frac{(1+w)^2}{1+2w}\right]+54\ln\tfrac{4}{3}(1+w)-8w-12\right] \ , \tag{3.24}$$

$$\eta^A=\tfrac{1}{18}(6\ln\tfrac{4}{3}-1)u^2=\tfrac{1}{50}(6\ln\tfrac{4}{3}-1)\epsilon^2=0.0145 \ , \tag{3.25}$$

$$P=-c_d f \ . \tag{3.26}$$

Equations (3.16) and (3.17) have corrections of order f^3, and f^2 times powers of v in the curly brackets, and Eq. (3.26) has corrections of order f^2, and f times powers of v. The constant c_d can be calculated using either a four-dimensional[13] or a three-dimensional[52] formalism, which represent different approximations to the real three-dimensional system. The respective values are

$$c_4=\tfrac{1}{4} \ , \tag{3.27a}$$

$$c_3=\tfrac{1}{2}-\tfrac{1}{8}\pi=0.107 \ , \tag{3.27b}$$

and we shall analyze the experimental data with both choices. Our final formula for λ is thus Eq. (3.13) with $\epsilon=1$, and $\hat{R}_\lambda$ given by

$$\hat{R}_\lambda(t)=(2\pi^2)^{-1/2}[f(l)w'(l)]^{-1/2}[1-c_d f(l)] \ . \tag{3.28}$$

The above theory constitutes a well-defined prescription for calculating the thermal conductivity λ in terms of the experimentally determined quantities g_b, ξ_0, ν, and C_P (cf. Table I), and the functions $f(l)$ and $w(l)$ obtained by solving (3.10) and (3.11). Thus, if v is obtained from the experimental C_P via (3.12), there are three unknown integration constants, f_0, w_0', and w_0'', representing initial values at some temperature. These correspond to the freedom of choosing the bare parameters λ_b and $\Gamma_b=\Gamma_b'+i\Gamma_b''$.

Equations (3.16)–(3.26), which define model F,[11]

are appropriate to liquid ^{4}He, in which the specific heat C_P has a singularity at T_λ. In Ref. 11 a simpler model was also discussed, the so-called symmetric model (E), in which C_P is constant. The equations for model E are obtained from model F by setting

$$v \equiv 0 \ , \tag{3.29}$$

$$w = w' ; \ w'' = 0 \ , \tag{3.30}$$

which implies $\tilde{h} = 0$ in (3.16) and (3.17). In applications of the theory to experiment it was suggested in Ref. 11 that one could calculate w and f using the model E equations, but insert the experimental (singular) specific heat in Eq. (3.13). This approximation, which has been adopted by other authors,[18,19,25] is a good one near the fixed point, but as shown below, it fails over a sizable portion of the experimental range. We shall denote the model with a constant C_P as "model E_0" and the phenomenological model with a singular C_P in (3.13) as "model E_s."

Let us end this subsection by reviewing the domain of validity of our theoretical prediction for the thermal conductivity. First of all we must discuss the validity of the model, and then how accurately we are calculating the thermal conductivity within the model. The question of the precise relationship between experimental quantities such as the thermal conductivty λ and corresponding calculated quantities, is a complicated one in general. One reason is because the physical quantities are the *bare* ones (in a theory with finite cutoff Λ_c), whereas the field-theoretic formalism[13,52,53] calculates the renormalized functions (with $\Lambda_c = \infty$). Near the critical point the distinction amounts to a multiplicative normalization factor, but away from T_c the relationship is more complicated. In order to make quantitative comparisons between experiment and theory we shall take the following phenomenological point of view: We assume that the renormalized functions represent the corresponding physical variables, i.e., the unknown normalization factor is adjusted at a given (high) temperature. Instead of being defined by the bare parameters λ_b, Γ_b, $\tilde{u}_b$, C_{Pb}, etc., the model will be characterized by the formal high-temperature limit of the corresponding renormalized parameters, e.g.,

$$\lambda_\infty = \lim_{l \to -\infty} \lambda(l) \approx \lambda_b \ . \tag{3.31}$$

It is these high-temperature limits λ_∞, Γ_∞, $C_{P\infty}$, etc., which we wish to identify with the "background" values extracted from analyses of experimental data.

If the background values were constant, this procedure would be quite unambiguous, but in fact they have a (smooth) temperature dependence coming from the variables which are not included in our starting model (first sound, quasiparticles, etc.). A more accurate starting point is therefore a model where the bare parameters are themselves (smooth) functions of temperature. It follows that this dependence will also manifest itself in the high-temperature limits such as (3.31). In Sec. IV C we shall analyze a model which takes account of such a smooth temperature dependence.

Concerning the purely static transients, the situation is rather favorable, since our formulas express the dynamics essentially exactly in terms of the static parameters C_P and κ. These formulas arose from a second-order expansion in the static couplings u and v, but it seems clear that apart from corrections of order of the static exponent[50] η, the theory can be reexpressed in terms of the *exact* C_P and κ. We shall take these quantities from experiment, the first from direct thermodynamic measurements,[42] and the second via scaling from the superfluid density.[36] Of course, Eq. (3.7) neglects the static transients, but the theory itself is expressed in terms of the functions $\kappa(t)$ and $C_P(t)$ which could, in principle, include all static transients.

Let us now turn to the question of the validity of our calculations within the model. We have used perturbation theory in the dynamic coupling constant f, so the theory is valid whenever f is small.[54] At the fixed point we have $f^* \sim 4 - d$, so the expansion is only valid for $d \approx 4$. It turns out,[23] however, that for arbitrary d, f is always small for temperatures sufficiently far from the critical point. How far depends on the bare coupling constant f_b, and for ^{4}He the remarkable fact is that $f(l)$ is already small above a reduced temperature $t_c \approx 10^{-3}$ (t_c depends on pressure and decreases with increasing pressure).

In summary, we can thus state that the theory is quantitatively correct for $t \gtrsim t_c$, but since f^* is without doubt of order unity in three dimensions, all powers of f are in principle needed for an exact critical theory (in the range $t \lesssim t_c$).

B. Fixed point and the weak-scaling instability

At the three-dimensional fixed point we must make an uncontrolled extrapolation of the small-f expansion to the domain $f = O(1)$. In the present problem there are essentially two methods available for this extrapolation; these are the usual ϵ expansion,[11,13,16,17] and a self-consistent method[18,52] which solves the truncated (nonlinear) equations for the fixed point directly in three dimensions. A comparison between the two methods has been given earlier,[18,52] and in view of the similarity of the results we shall use the more convenient self-consistent method to find f^* and w^*. These are obtained by solving the equations

$$\beta_w(f^*, w^*) = 0 \ , \tag{3.24a}$$

$$\beta_f(f^*, w^*) = 0 \ . \tag{3.32b}$$

The results as a function of d were presented in Ref. 18, where it was found that for $d=3$

$$f^*=0.827, \quad w^*=0.018 \ , \tag{3.33}$$

i.e., the model is almost at the instability point for dynamic scaling ($w^*=0$), which occurs here for $\epsilon^*=4-d^*\approx 1.02$. For lower dimensionality, one has *weak scaling,*[13] for which Eq. (3.13) must be modified, as discussed elsewhere.[13,18]

In view of the proximity of the result (3.33) to the weak-scaling instability, it is interesting to explore the effect of the truncation of Eqs. (3.16) and (3.17) on the answers. We have done this in an *ad hoc* way, by adding the term

$$-B_3 w f^3 \tag{3.34}$$

with B_3 a constant, to the right-hand side of (3.17), leaving (3.16) unchanged. The ensuing values of ϵ^* and w^* ($\epsilon=1$) as a function of B_3, obtained from (3.32) are shown in Figs. 6(a) and 6(c), and show a surprisingly large variation for values of B_3 less than unity. In fact, with our particular choice of a B_3 which is w independent, we find that for $B_3>0.16$ there is no more weak-scaling instability for any d near 3. This is shown in Fig. 6(b), where the minimum value of $w(l)$ (minimized over ϵ and l for fixed B_3) is shown as a function of B_3. The corresponding value of ϵ is shown in Fig. 6(a) (right-hand scale). Although the above results are only suggestive and are not to be taken literally, they show that a modest contribution from higher-order terms in (3.16) and (3.17) can change the quantitative picture at the fixed point. Nonetheless, it is reasonable to assume that the value of w^* will be small in three dimensions, so that the arguments given earlier[13–21] about the importance of transients will still come into play.

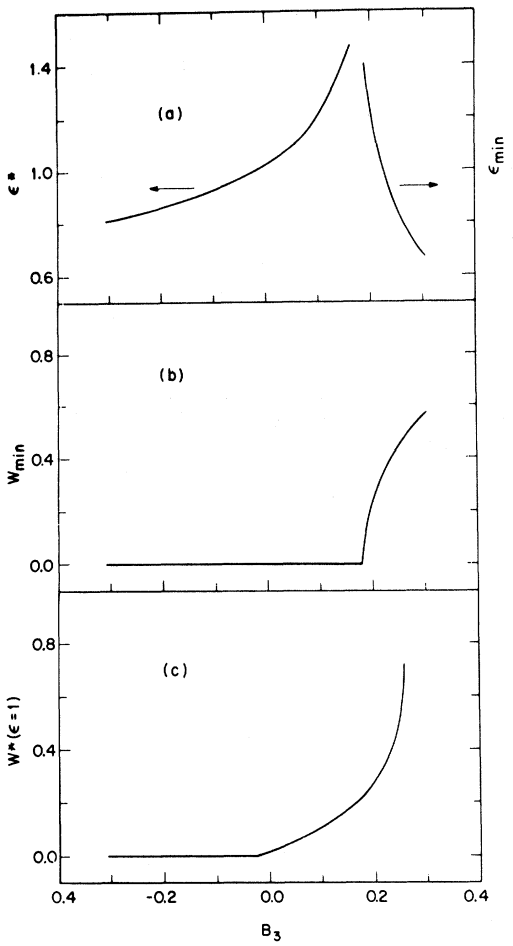

FIG. 6. Effect of the phenomenological three-loop term with coefficient B_3 [Eq. (3.34)], on the fixed-point parameters of the theory. In (a) the left-hand curve gives the dimensionality $d^*=4-\epsilon^*$ for breakdown of dynamic scaling ($w^*=0$), and the right-hand curve gives the ϵ value at which w reaches its (positive) minimum when dynamic scaling does not break down. Part (b) shows this minimum value of w (minimized over ϵ and l), and part (c) gives the value of w^* for $d=3(\epsilon=1)$.

C. Behavior at high t

A limit in which our models have simple behavior is $t\to\infty$ (or $\kappa\to\infty$), where it turns out that perturbation theory is valid for all d. Let us first discuss this limit from a purely formal point of view and then consider its physical relevance. For simplicity we discuss model E_0 ($C_P=C_{Pb}$). We rewrite Eqs. (3.10), (3.11), (3.16), and (3.17) in the form ($\tilde{h}=0$)

$$\frac{\kappa}{f}\frac{df}{d\kappa}=-1+f\left(\frac{1}{2}+\frac{1}{1+w}\right)+O(f^2) \ , \tag{3.35a}$$

$$\frac{\kappa}{w}\frac{dw}{d\kappa}=f\left(\frac{1}{2}-\frac{1}{1+w}\right)+O(f^2) \ , \tag{3.35b}$$

where we are using the variable κ [Eq. (3.6)], and we have set $\eta^A=0$ for the moment. In the limit $\kappa\to\infty$ we set

$$\tilde{f}\equiv f\kappa=\tilde{f}_\infty[1+\tilde{f}_1\kappa^{-1}+O(\kappa^{-2})] \ , \tag{3.36}$$

$$w=w_\infty[1+w_1\kappa^{-1}+O(\kappa^{-2})] \ , \tag{3.37}$$

and find

$$\tilde{f}_1=-\tilde{f}_\infty\left(\frac{1}{2}+\frac{1}{1+w_\infty}\right) \ , \tag{3.38}$$

$$w_1=-\tilde{f}_\infty\left(\frac{1}{2}-\frac{1}{1+w_\infty}\right) \ , \tag{3.39}$$

with $\tilde{f}_\infty$ and w_∞ constants of integration. Thus the

coupling constant $f \equiv \tilde{f}\kappa^{-1}$ behaves as

$$f = \frac{\tilde{f}_\infty}{\kappa}\left[1 + \frac{\tilde{f}_1}{\kappa} + O(\kappa^{-2})\right] , \tag{3.40}$$

i.e, it vanishes at high temperatures. The thermal conductivity in model E_0 is given in Eqs. (3.13) and (3.15), and has the form

$$\lambda = \lambda_\infty\left[1 + \frac{\lambda_1}{\kappa} + O(\kappa^{-2})\right] , \tag{3.41}$$

$$\lambda_\infty = g_b(C_{Pb}\xi_0 K_d/\tilde{f}_\infty w_\infty)^{1/2} , \tag{3.42}$$

$$\lambda_1 = \tilde{f}_\infty(\tfrac{1}{2} - c_d) , \tag{3.43}$$

where C_{Pb} in (3.42) is the constant value of C_P. Note that the correction P [Eqs. (3.15) and (3.26)] affects the first-order term λ_1, whereas it only enters in second order near the fixed point.[11] In the three-dimensional theory[52]

$$c_d = \tfrac{1}{2} - \tfrac{1}{8}\pi ,$$

so

$$\lambda_1 = \tfrac{1}{8}\tilde{f}_\infty\pi , \tag{3.44}$$

in agreement with the calculation of Ref. 55 (see Appendix A).

Model F may be analyzed in the same way, but care must be taken to treat the specific-heat singularity consistently. In particular, the experimental specific heat[42,47] has a minimum above T_λ, which leads to an effective exponent α_e, Eq. (3.12), which becomes negative at that point, so that our Eq. (3.5) cannot be used. We believe that this minimum in C_P is due to regular terms, which should not contribute to the vertex v defined in (3.5) and (3.12). In order to obtain a usable v we have, somewhat arbitrarily, replaced the effective exponent calculated from the experimental C_P by a function which goes to zero smoothly at high temperatures and remains positive. The specific heat obtained from this function by integrating (3.12) then represents an approximation to the *singular* part of the physical specific heat. This procedure, which is illustrated in Fig. 7 and described in more detail in Appendix A, is the one we will always use in what follows.

Having a function v which is everywhere positive, we may now integrate model F out to high temperatures. In Appendix B it is shown analytically that the first-order result for the thermal conductivity at high temperatures, Eq. (3.41), remains *unchanged* in model F. This comes about because the κ^{-1} corrections to C_P precisely cancel the change in the behavior of $w(\kappa)$ and $f(\kappa)$ resulting from the v terms in (3.17) and (3.18) [the constant C_{Pb} in (3.42) is replaced by the high-temperature limit $C_{P\infty}$ of the specific heat].

The phenomenological model E which inserts the

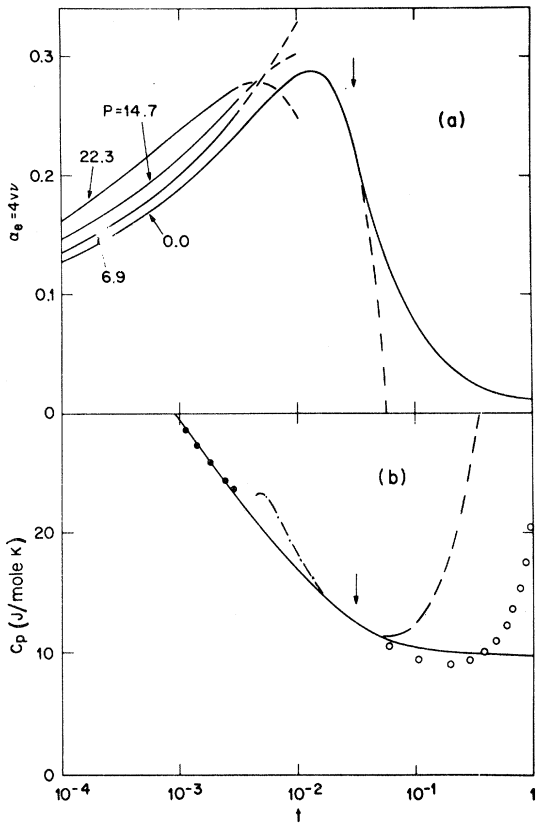

FIG. 7. (a) Effective exponent α_e of the specific heat [Eq. (3.12)] vs reduced temperature. The curves are obtained by differentiating the experimental specific heat given by Eq. (2.7), with parameters listed in Table I for the different pressures. The dashed lines are extrapolations beyond the range where the specific-heat data were used to obtain (2.7). The solid line extending the $P=0$ curve to high temperatures is Eq. (A3), as discussed in Appendix A. (b) The specific heat C_P obtained by integration of the α_e ($P=0$) curve in part (a). The solid and dashed lines are obtained from the corresponding curves in part (a) for $P=0$, and the dot-dashed line is obtained from Eq. (A4). The solid circles are C_P data from Ref. 42 and the open circles come from Ref. 47 (see Table III).

singular specific heat into (3.13) but sets $v=0$ in (3.17) and (3.18) (model E_s) has a high-temperature limit of the form

$$\lambda = \lambda_\infty\left[1 + \frac{\lambda_1}{\kappa} + O(\kappa^{-2})\right]\left[\frac{C_P}{C_{P\infty}}\right]^{1/2} , \tag{3.45}$$

which is quite far from the correct answer for parameters appropriate to ^{4}He. A comparison between models E_0, E_s, and F is shown in Fig. 8, where it is seen that model E_0 is a good approximation to F at high temperatures whereas E_s is better near the fixed point.

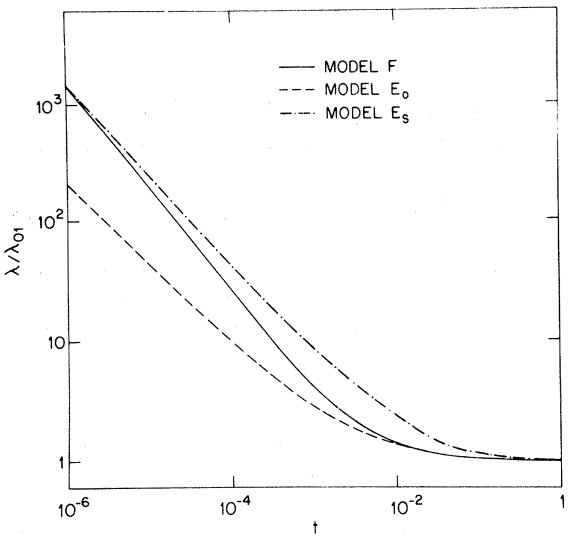

FIG. 8. Thermal conductivity λ (normalized by its $t=1$ value) vs reduced temperature on log-log scales. The parameters are typical ones for ^{4}He, namely, $c_d=0.107$, $\tilde{f}_\infty=2.14\times10^{-2}$, $w'_\infty=0.493$, and for model F, $w''_\infty=-0.220$. The three models are defined in Sec. III A and involve different treatments of the specific-heat singularity.

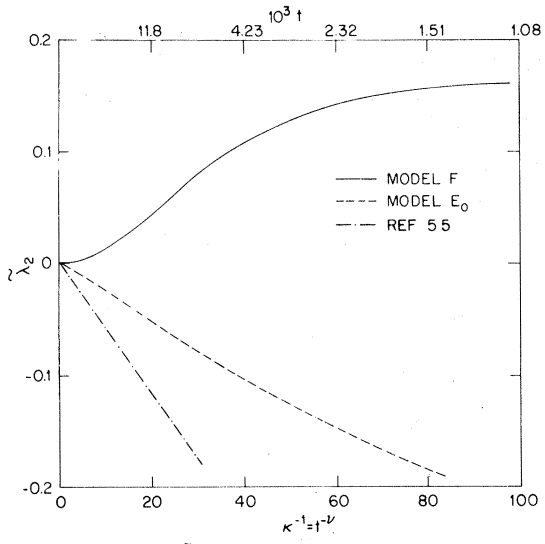

FIG. 9. Function $\tilde{\lambda}_2(\kappa)$ defined in Eq. (3.46), as a function of $\kappa^{-1}=t^{-\nu}$. The parameter values are the same as in Fig. 8, but in addition the quantity η^A, Eq. (3.25), is set equal to zero. The dot-dashed curve has the same $\tilde{f}_\infty$ and w_∞, and corresponds to the asymptotic value obtained for model E_0 in Ref. 55. The top scale gives the reduced temperature.

The analysis of Appendix B shows that the second-order correction to λ and the $O(\kappa^{-1})$ term in $\tilde{f}$ will be different in models E and F. Indeed, if we define $\tilde{\lambda}_2(\kappa)$ as the deviation from the first-order approximation, i.e.,

$$\lambda\equiv\lambda_\infty\left[1+\frac{\lambda_1}{\kappa}[1+\tilde{\lambda}_2(\kappa)]\right] , \tag{3.46}$$

then it turns out that $\tilde{\lambda}_2$ does not vary linearly in κ^{-1} in model F, over an appreciable range of κ. In any case, models F and E_0 give different answers, as shown in Fig. 9 where $\tilde{\lambda}_2$ is extracted from a numerical integration of our model F with parameters appropriate to ^{4}He. It must be noted, however, that our equations do not give $\tilde{\lambda}_2$ exactly for either model, in view of the absence of the f^2 terms in our expansion for P, Eq. (3.26). In Appendix B we have extracted $\tilde{\lambda}_2$ from the calculation of Ref. 55, which is claimed to be exact to second order in κ^{-1} (this calculation is appropriate to model E_0 if we set $C_P\equiv C_{Pb}$). The result is also indicated in Fig. 9 and the slope differs by a factor of 2 from our model E_0 answer. We see no reason, however, to assume that the correct $\tilde{\lambda}_2$ in model F will be well approximated by either model E_0 or E_s, or by the approximate treatment of Ref. 55 (see Appendix B). For our purposes, we consider Fig. 9 to give a reasonable estimate of the size of $\tilde{\lambda}_2$, in order to define the domain of validity of the expansion.

The physical relevance of the high-temperature expansion comes entirely from the fact that it is an expansion in κ_c/κ rather than in κ^{-1}. Moreover, as shown in Sec. IV B below, in ^{4}He $\kappa_c=\lambda_1=\frac{1}{8}\tilde{f}_\infty\pi$ *is a small parameter*[56] *of order* 10^{-2}. The situation is thus analogous to that which occurs in superconductivity, where there is a large Aslamazov-Larkin[57] region where weak-coupling methods apply ($\kappa_c\lesssim\kappa\ll1$). In that case the small parameter is k_BT_c/E_F, whereas here its physical origin in the bare theory is more obscure.

D. Nonlinear behavior

Having discussed the fixed-point ($\kappa\to0$, $l\to+\infty$) and high-temperature ($\kappa\to\infty$, $l\to-\infty$) limits of the model, let us study the nonlinear evolution between the two regimes, as a function of the initial values. These are the only unknown parameters left in the problem and they determine the constants λ_∞, w_∞, and $\tilde{f}_\infty$ of Eqs. (3.41)–(3.43), but they drop out of the fixed-point values w^* and f^*. We shall in general denote the initial values of w and f at the arbitrary temperature t_0 in Eq. (3.6), by[49]

$$w(l=0)\equiv w_0=w'_0+iw''_0 , \tag{3.47}$$

$$f(l=0)\equiv f_0 . \tag{3.48}$$

Let us study the behavior of the model as a function of the initial values for the choice $t_0=1$,

$$t_0=1;\ \kappa=1,\ w_0=w_{01};\ f_0=f_{01}=\tilde{f}_{01} , \tag{3.49}$$

which we consider to be reasonable approximations

to the bare values w_b and f_b. (We shall discuss the question of regular transients in Sec. IV C below.) For the present purposes, it is sufficient to consider model E_0, for which

$$v=0, \quad w''=0 \ , \tag{3.50}$$

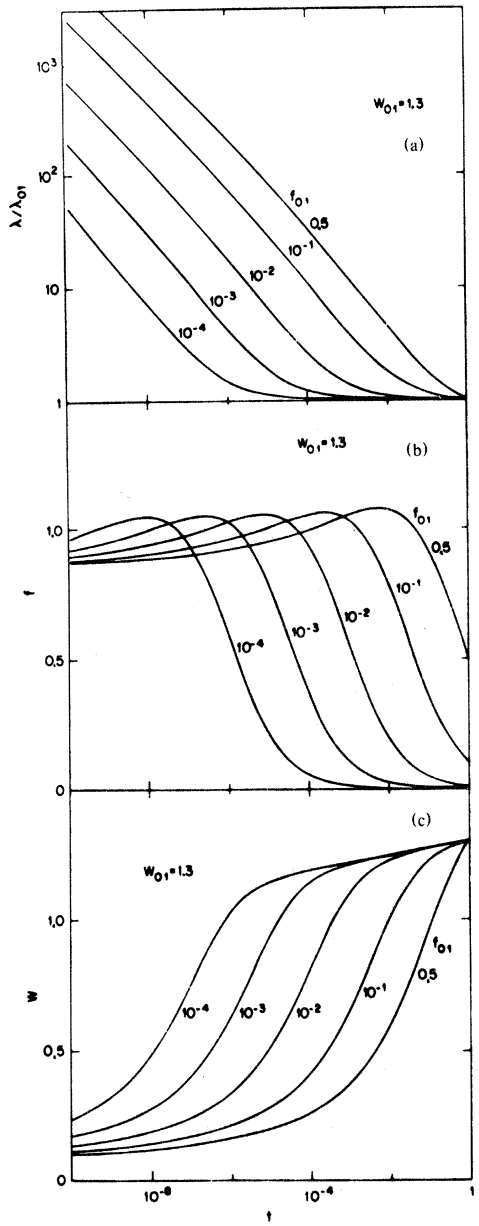

FIG. 10. Numerical study of model E_0 equations for different values of the initial condition f_{01} of the coupling constant $f(t)$ at $t=1$, for fixed initial value w_{01} of the ratio $w(t)$ at $t=1$. Although the fixed-point ($t\to 0$) is the same in all cases, the crossover from high-temperature to critical behavior occurs at a reduced temperature t_c which depends strongly on f_{01}. Part (a) shows the thermal conductivity λ, part (b) the coupling constant f, and part (c) the frequency ratio w.

and

$$\lambda=\lambda_0(2\pi^2 wf\kappa)^{-1/2}(1-c_3 f) \ , \tag{3.51}$$

where $c_3=0.107$ [Eq. (3.28)], and λ_0 is a constant which need not concern us here. For the particular choice (3.49), we have

$$\lambda_{01}=\lambda_0(2\pi^2 w_{01}f_{01})^{-1/2}(1-c_3 f_{01}) \ . \tag{3.52}$$

Our analysis of the experimental thermal conductivity to be described in Sec. IV shows that typical values of the parameters w_{01} and f_{01} which lead to a model E fit are

$$w_{01}=1.3, \quad f_{01}=0.01 \ , \tag{3.53}$$

leading to $\lambda_{01}/\lambda_0=1.95$. We have therefore integrat-

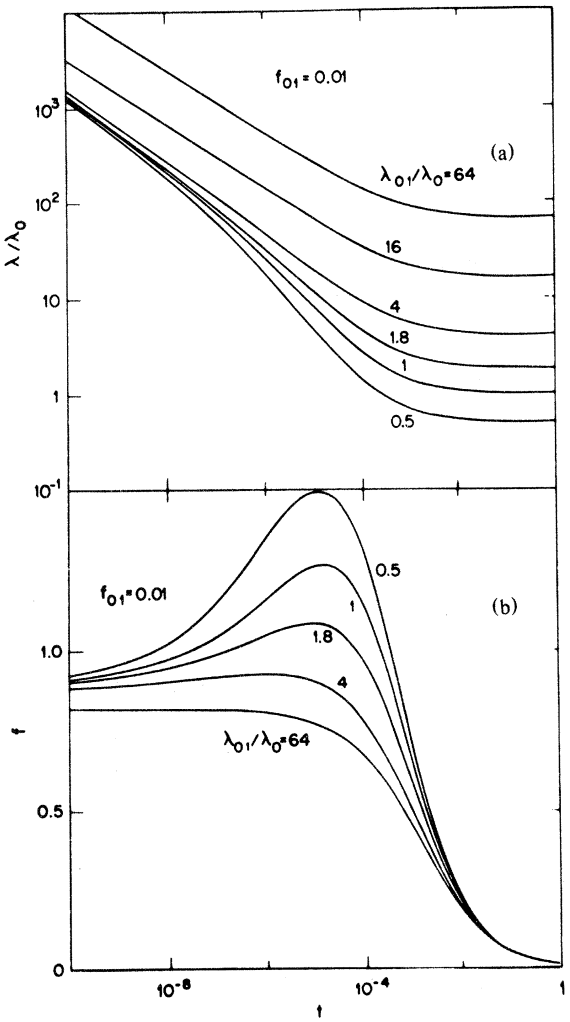

FIG. 11. (a), (b) Behavior of model E_0 for fixed initial coupling constant f_{01} and varying initial value λ_{01} of λ at $t=1$. The crossover temperature from "background" to critical behavior is seen to be independent of λ_{01}. The quantity λ_0 is an arbitrary normalization constant.

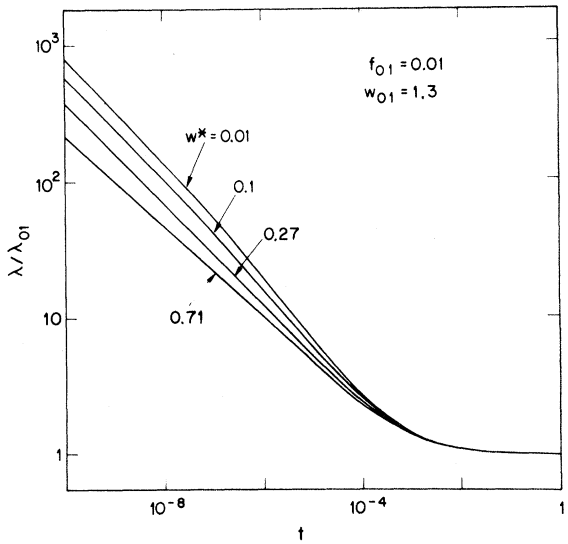

FIG. 12. Dependence of the thermal conductivity in model E_0 on the fixed-point value w^*, for fixed initial values of f_{01} and w_{01}. The value of w^* was varied by inclusion of the three-loop term (3.34), as illustrated in Fig. 6. The crossover temperature t_c is independent of w^*, which only influences the effective exponent in the critical region $t < t_c$.

ed the model E_0 equations numerically, for $t < t_0$, using various initial conditions at $t_0 = 1$, which vary around the typical values (3.53). The numerical results were generally well behaved, though for some values of initial parameters instabilities appeared. Since these occurred for choices which were rather far from the physical values (3.53), we did not investigate these phenomena further. In Fig. 10 we vary f_{01} at fixed w_{01} and study the temperature dependence of the three quantities λ, f, and w on a wide temperature range. It is seen that the crossover from high-t to fixed-point behavior moves in as f_{01} is decreased. In Fig. 11, on the other hand, f_{01} is fixed and w_{01} varied, in such a way that λ_{01} [Eq. (3.52)] is changed. For this case the crossover temperature remains roughly constant, and only the shape of the curves changes. In Fig. 12 we include the phenomenological three-loop term (3.34) in the model, and thereby change the value of w^*, leaving f_{01} and w_{01} the same. The values of λ are only modified significantly for $t < 10^{-4} \sim 10^{-5}$, and the crossover temperature is quite independent of w^*. Finally, in Fig. 13 we repeat the calculation of Fig. 10(a) using model F, with a reasonable starting value of the imaginary part, $w_{01}'' = -0.2$.[58] The behavior is seen to be qualitatively similar to that in model E_0. The present study thus demonstrates unambiguously that the small dynamic crossover temperature in ^{4}He results from a weak bare coupling constant ($f_{01} \approx f_b$), and not from a large background λ,[19] or from a small w^*,[19,25] as previously claimed.

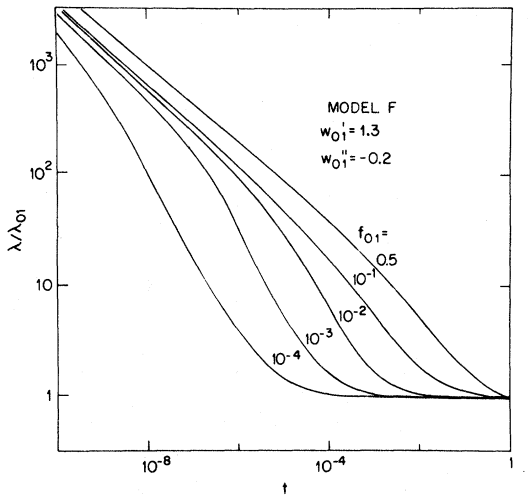

FIG. 13. Calculation of Fig. 10(a) repeated for model F, which includes the singular specific heat, and the imaginary part of the ratio w. The crossover behavior is qualitatively the same as in Fig. 10(a).

IV. ANALYSIS OF EXPERIMENTAL DATA

Having elucidated the qualitative features of the theory, we shall apply it to the experimental data in order to test its predictions, and to extract nonuniversal parameters from experiment. In each case we have compared the theoretical predictions for $\hat{R}_\lambda(t)$, Eq. (3.15), with the experimental $\hat{R}_\lambda(t)$ discussed in Sec. II.

A. Power-law fits

We shall first discuss a number of traditional power-law analyses, in order to test various earlier results[19] and suggestions.[18] The two theoretical forms we shall consider are

$$\hat{R}_\lambda^2 = (2\pi^2)^{-1}\frac{C_\lambda}{(x_1/\nu)}(1-t^{x_1}) + R_{1\lambda}t^{x_1} + R_{3\lambda}t^{x_3} \quad . \tag{4.1}$$

and

$$\hat{R}_\lambda = \left[\frac{C_\lambda}{2\pi^2(x_1/\nu)}\right]^{1/2}(1 - R_{1\lambda}t^{x_1} + R_{3\lambda}t^{x_3}) \quad . \tag{4.2}$$

Equation (4.1) (the "quadratic" approximation) was suggested by Hohenberg *et al.*[18] since it represents the exact asymptotic behavior of model E in the limit $x_1 \propto w^* \to 0$. The "linear" approximation, Eq. (4.2) was employed by Ferrell and Bhattacharjee[19] to fit the thermal conductivity, but in contrast to (4.1) it does not remain finite in the limit $x_1 \to 0$, $t \neq 0$. Both forms (4.1) and (4.2) were shown by Dohm and Folk[25] to be inaccurate approximations to the exact

model E behavior over the whole temperature range $10^{-6} < t < 1$ (the quadratic approximation was found to be rather accurate for $10^{-6} < t < 10^{-3}$).

In order to test these expressions we have carried out fits of the experimental $\hat{R}_\lambda$ values to Eqs. (4.1) and (4.2) for $t < 3 \times 10^{-3}$, treating $R_{1\lambda}$ and $R_{3\lambda}$ as adjustable, and assuming C_λ and x_1 to be either adjustable or fixed by theory.[18] The results are shown in Fig. 14 for cell A, and in Table IV for cells A and D. An examination of the numbers obtained suggests that a power-law fit over a restricted range gives limited quantitative information on the physical parameters. Indeed, if one fixes the universal quantities C_λ and x_1 from theory, as in fits 1, 3, 5, and 7 of Table IV one obtains a rather poor fit to the data, as indicated by the deviation σ. If one lets C_λ and x_1 be determined by the data (fits 2, 4, 6, and 8 of Table IV) the fit improves markedly, but the values obtained for C_λ and x_1 are rather far from the expected values[18] (especially for the quadratic case). These results could be interpreted as favoring the linear fit (4.2), but such a conclusion seems to us erroneous for the following reasons: Firstly, as noted also by Dohm and Folk,[25] the values of the correction amplitudes $R_{1\lambda}$ and $R_{3\lambda}$ obtained in the fits are rather large (see Table IV), whereas one would *a priori* expect them both to be of order unity. Secondly, expressions (4.1) and (4.2) are approximations to model E, and one may ask how accurate the model itself is in this temperature range. The answer to be given in Sec. IV B is that model E (more precisely model E_s, see Sec. III A) does not fit the data very well for $10^{-6} < t < 3 \times 10^{-3}$. A model E_s fit is shown in Fig. 14(a) for comparison (the initial values f_0 and w_0 were adjusted at $t_0 = 3 \times 10^{-3}$), and the result is only slightly better than the quadratic approximation; it is in fact worse than the linear approximation [curve 3 in Fig. 14(b)]; these comparisons are meaningful since each of the fits has two adjustable parameters.

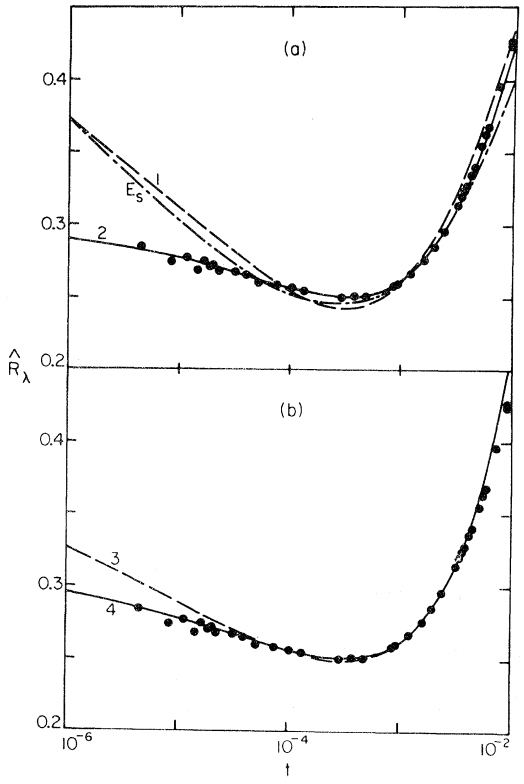

FIG. 14. Power-law fits (dashed lines) of the data in cell A to (a) Eq. (4.1) and (b) Eq. (4.2) in the range $t < 0.003$, treating the correction amplitudes $R_{1\lambda}$ and $R_{3\lambda}$ as adjustable. The solid lines have the leading amplitude C_λ and the correction exponent x_1 in (4.1,2) as additional adjustable parameters. The numbers on the curves (1–4) refer to entries in Table IV, where the values of the parameters are listed. The curve marked E_s in part (a) is a nonlinear model E_s fit analogous to the ones in Fig. 17 below, but for $t < 0.003$, and is shown for comparison.

TABLE IV. Power-law fits to Eqs. (4.1) ("quadratic") and (4.2) ("linear"), with $t_{max} = 3 \times 10^{-3}$.

Fit	Cell	Type	C_λ	x_1	x_3	$R_{1\lambda}$	$R_{3\lambda}$	$10^3\sigma$
1	A	Quad.	0.62[a]	0.010[a]	0.533[a]	−0.16	2.91	8.5
2	A	Quad.	1.16	0.45	0.533[a]	−6.02	10.07	0.9
3	A	Lin.	0.63[a]	0.068[a]	0.648[a]	1.08	12.17	2.7
4	A	Lin.	0.82	0.29	0.648[a]	3.64	28.98	0.9
5	D 0.0	Quad.	0.62[a]	0.010[a]	0.533[a]	−0.13	2.41	2.3
6	D 0.0	Quad.	0.77	0.10	0.533[a]	−0.24	2.61	1.2
7	D 0.0	Lin.	0.63[a]	0.068[a]	0.648[a]	0.95	8.60	3.8
8	D 0.0	Lin.	1.03	0.038	0.648[a]	1.02	6.45	1.2

[a]Parameter held constant in the fit.

The general conclusion we draw from these power-law fits is that their quality says little about the correctness of the starting expressions, and that the parameter values they yield are not physically meaningful. At the very best, these fits can be considered as a purely empirical representation of the data over a limited temperature range.

B. Nonlinear fits

1. Estimate of bare parameters

Let us first estimate the bare parameters of our model from the "background values" (or high-temperature extrapolations) of λ and C_P, and from the mode-coupling constant g_b. At vapor pressure the data in Fig. 5 extrapolate to roughly 1400 erg/cm sec K at high t, which (dividing by k_B) yields[39]

$$\lambda_b = 10^{19}\ (\text{cm sec})^{-1} \ . \tag{4.3}$$

For C_{Pb} we take the minimum value 10 J/mole K, which must be divided by the molar volume $V = 27.4\ \text{cm}^3/\text{mole}$ and k_B to yield

$$C_{Pb} = 2.6 \times 10^{22}\ \text{cm}^{-3} \ . \tag{4.4}$$

Thus the background thermal diffusivity is

$$\lambda_b / C_{Pb} = 3.8 \times 10^{-4}\ \text{cm}^2/\text{sec} \ . \tag{4.5}$$

The mode-coupling constant is (see Table I)

$$g_b = \sigma_\lambda k_B T_\lambda / \hbar = 2.13 \times 10^{11}\ \text{sec}^{-1} \ . \tag{4.6}$$

To find w_b and f_b Eqs. (3.2) and (3.3) we still need the order parameter diffusivity Γ_b, which is not known, but we expect[19]

$$\Gamma_b = (\hbar / m_{\text{He}})\tilde{\Gamma}_b = 1.56\tilde{\Gamma}_b \times 10^{-4}\ \text{cm}^2/\text{sec} \ , \tag{4.7}$$

with $\tilde{\Gamma}_b$ of order unity. According to Eqs. (4.3)–(4.7) we thus have

$$w_b = \frac{\Gamma_b C_{Pb}}{\lambda_b} = 0.42\tilde{\Gamma}_b \tag{4.8}$$

and

$$\tilde{f}_b = f_b \kappa = \frac{g_b^2 \xi_0}{2\pi^2 \lambda_b \Gamma_b} = 0.02\tilde{\Gamma}_b^{-1} \ , \tag{4.9}$$

where we have used $\xi_0 = 1.4$ Å. We thus see that if $\tilde{\Gamma}_b$ is of order unity the bare coupling constant will be of order 10^{-2}, whereas w_b will be of order unity. This means that the crossover temperature is $t_c \approx 10^{-3}$ (see Fig. 10), so that the high-temperature limit discussed in Sec. III C will have been reached at $\kappa = 1$, and the constants $\tilde{f}_\infty$, λ_∞, and w_∞ are well approximated by their values at $\kappa = 1$. Comparing the curve for λ marked $f_{01} = 0.01$ in Fig. 10(a) to the experimental data shown in Fig. 15, we already see that the theory predicts the overall temperature dependence of λ semiquantitatively over five decades, without adjustable parameters other than a normalization at $t = O(1)$. In the remainder of this section we shall make more quantitative tests of the theory, and attempt to extract reliable values of the parameters.

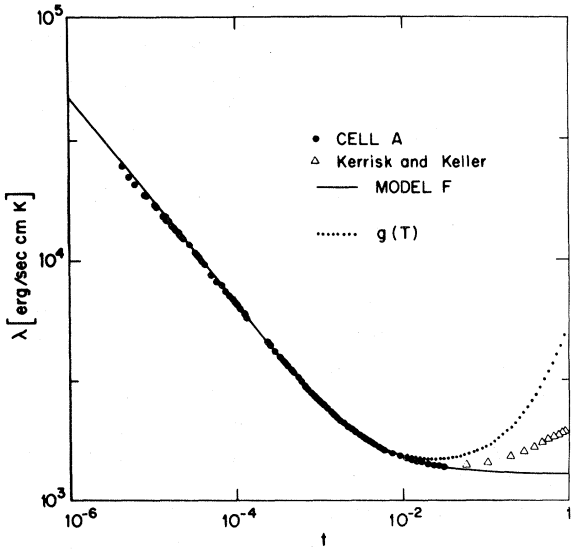

FIG. 15. Thermal conductivity in cell A (solid circles) vs reduced temperature (on log-log scales), along with the data of Kerrisk and Keller (Ref. 33, open triangles). The solid line is a fit using model F with four adjustable parameters in the range $10^{-6} < t < 10^{-2}$, namely, f_0, w_0', w_0'', and B_3 (see entry 3 of part b of Table VI). The dotted line is obtained by using $g_b(T)$, Eq. (4.12) in the formula for $\hat{R}_\lambda$ (2.1) in place of g_b.

2. Limited-range fits

In order to test the different models we shall fit the data over a limited temperature range selected so that regular transients are unimportant, while at the same time the coupling f is small. Having determined the parameters from this fit, we then integrate the equations outside of the limited range, and compare the resulting $\hat{R}_\lambda$ [Eq. (3.28)] with experiment. We have chosen the range

$$0.003 < t < 0.01 \ , \tag{4.10}$$

and have used the data from cell A. The parameter t_0 was chosen at $t_0 = 0.01$ and the adjustable parameters were $w_0 = w_0'$ and f_0 for model E_s, and w_0', w_0'', and f_0 for model F.

The fits were obtained by (i) integrating the equations numerically with given initial values, (ii) evaluating the deviations between experiment and

theory, and (iii) adjusting the initial values so as to minimize the squared deviations. The fits yielded the best values of the adjusted parameters, the probable errors in these quantities, and the deviation σ from the fit, expressed as the square root of the variance

$$\sigma=\left[\left(\frac{N}{N-K}\right)\sum_{i=1}^{N}(R_{\lambda i}^{\text{expt}}-R_{\lambda i}^{\text{theor}})^2 W_i/\sum_{i=1}^{N} W_i\right]^{1/2}, \tag{4.11}$$

where W_i is the weight attached to point i (see Sec. II B), N is the number of data points, and K the number of adjustable parameters. In carrying out such nonlinear fits with a number of parameters it is important to initiate the process with fairly accurate starting values, so as to converge in a reasonable number of steps (a typical run with two adjustable parameters would require 5 to 10 iterations, but runs with 4 parameters might involve 25 or more iterations).

Results of limited-range fits are shown in Fig. 16 for both model E_s and model F. It is seen that the model E_s curve deviates from the data as soon as one goes outside the range of fit, whereas the model F curve continues to agree for almost a decade on either side. More significantly, the deviations in model E_s occur for values of f (also shown in Fig. 16) which are small, and for which the perturbation expansion should be valid. For model F, on the other hand, the deviations occur only when f is of order unity, where the truncation errors in Eqs. (3.16), (3.17), and (3.26) cannot be neglected. Quantitative information on the limited-range fits is given in the tables[59] (entries 1 of parts a and b of Tables V and VI and entry 5 of Table VII).

Figure 16 also shows an interesting difference between model E_s and model F, in that $w'=w$ is monotonic in the former but w' has a maximum in the latter. This difference in behavior is quite general, and can be traced to the effect of the term $4v$ in

TABLE V. Fit of $\hat{R}_\lambda$ [Eq. (2.1)] to the predictions of model E_s [C_P from Eq. (2.7) $v\equiv 0$, $w''\equiv 0$], for two values of the constant c_d in Eq. (3.28). The range of data used in the fit is indicated in column 3, and the values of the parameters at $t=t_0$ are in columns 6 and 7. The constant B_3 is the phenomenological three-loop term, Eq. (3.34). The standard deviation σ of the fit is defined in Eq. (4.11).

Fit	Cell	Range	t_0	B_3	w_0	f_0	$10^3\sigma$
			(a) $c_d=c_4=0.25$				
1	A	$0.003<t<0.01$	10^{-2}	0[a]	1.454	0.171	2.0
2	A	$t<10^{-2}$	10^{-2}	0[a]	0.746	0.332	6.6
3	A	$t<10^{-2}$	10^{-2}	−0.056	0.799	0.310	6.1
4	D 0.0	$t<10^{-2}$	10^{-2}	0[a]	0.570	0.428	7.4
5	D 0.0	$t<10^{-2}$	10^{-2}	−0.072	0.649	0.367	5.0
6	A	$t<10^{-3}$	10^{-3}	0[a]	0.734	0.366	3.7
7	D 0.0	$t<10^{-3}$	10^{-3}	0[a]	0.491	0.838	1.4
8	D 6.9	$t<3\times10^{-4}$	10^{-3}	0[a]	0.658	0.802	0.9
9	D 14.7	$t<3\times10^{-4}$	10^{-3}	0[a]	0.716	0.660	1.1
10	D 22.3	$t<5\times10^{-4}$	10^{-3}	0[a]	0.844	0.521	1.8
11	A	$t<0.003$	10^{-2}	0[a]	0.735	0.368	3.4
			(b) $c_d=c_3=0.107$				
1	A	$0.003<t<0.01$	10^{-2}	0[a]	2.169	0.122	2.0
2	A	$t<10^{-2}$	10^{-2}	0[a]	1.066	0.260	6.5
3	A	$t<10^{-2}$	10^{-2}	−0.015	1.084	0.255	6.5
4	D 0.0	$t<10^{-2}$	10^{-2}	0[a]	0.809	0.344	6.1
5	D 0.0	$t<10^{-2}$	10^{-2}	−0.056	0.862	0.316	5.3
6	A	$t<10^{-3}$	10^{-3}	0[a]	0.922	0.674	5.1
7	D 0.0	$t<10^{-3}$	10^{-3}	0[a]	0.698	0.775	1.9
8	D 6.9	$t<3\times10^{-4}$	10^{-3}	0[a]	0.938	0.695	1.0
9	D 14.7	$t<3\times10^{-4}$	10^{-3}	0[a]	1.019	0.564	1.4
10	D 22.3	$t<5\times10^{-4}$	10^{-3}	0[a]	1.197	0.435	1.3
11	A	$t<0.003$	10^{-2}	0[a]	1.055	0.282	4.7

[a]Parameter held constant in the fit.

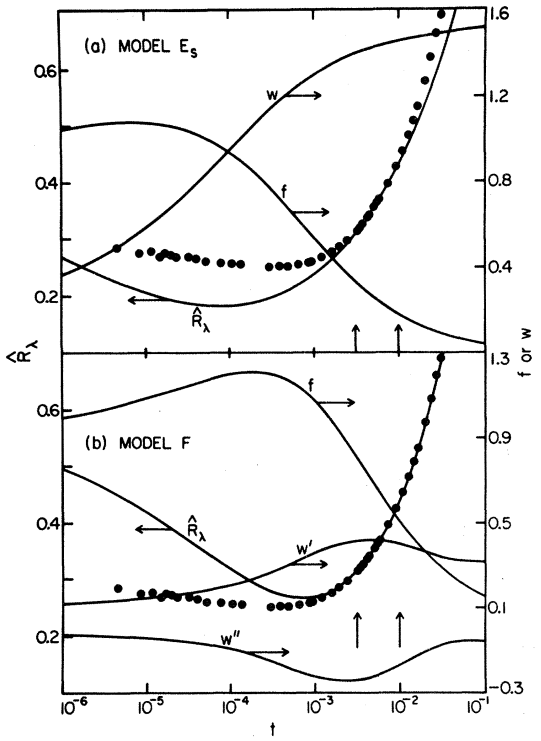

FIG. 16. Fits of the effective amplitude $\hat{R}_\lambda$ for cell A to (a) model E_s and (b) model F using data in the limited range $0.003 < t < 0.01$, between the vertical arrows. The theoretical curves for $\hat{R}_\lambda(t)$, $f(t)$, and $w(t) = w'(t) + iw''(t)$ so obtained have been extended to the full temperature range of the data. The fits correspond to entry 1 in part a Table V for (a) of the figure and entry 1 of part a of Table VI for part (b) of the figure.

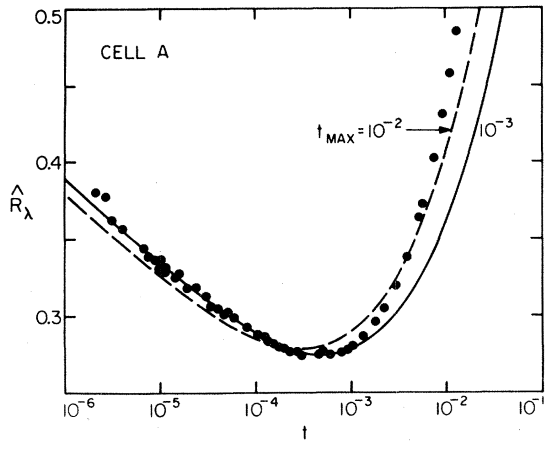

FIG. 17. Least-squares fit of $\hat{R}_\lambda$ in cell D to model E_s in the range $t < t_{max}$ for $t_{max} = 10^{-2}$ (dashed line) and $t_{max} = 10^{-3}$ (solid line). The adjustable parameters are f_0 and w_0 at $t = t_{max}$ and their values are shown in entries 4 and 7 in part b of Table V.

Eq. (3.17), which dominates at high temperatures and comes in with opposite sign from the contribution of f. Thus model E is qualitatively incorrect above the temperature of the maximum in w'.

3. *Fits over a large temperature range*

We have repeated the previous analysis including data over a larger temperature range, which was either $10^{-6} < t < 10^{-3}$ or $10^{-6} < t < 10^{-2}$. Let us first describe the analysis with model E_s at vapor pressure. Results for cell D with $t_{max} = 10^{-2}$ and $t_{max} = 10^{-3}$ were presented in Fig. 1(a) of Ref. 23, with an erroneous fitting procedure,[23] and the corrected results are shown in Fig. 17 of the present paper. The new curves still support the earlier contention that a satisfactory model E_s fit is only obtained for a limited portion of the data. Quantitative information on the fits for cells A and D is given in the tables, in entries[59] 2, 4, 6, and 7 in part a of Table V and entries 2, 4, 6, and 7, in part b of Table V from which it is seen that the deviation σ increases when t_{max} is extended from 10^{-3} to 10^{-2}.

Turning to model F, results of fits over the range $10^{-6} < t < 10^{-2}$ are given in entries 2 and 4 in parts a and b of Table VI and also show preceptible deviations from the data, despite the addition of the adjustable parameter w_0''. We attribute these deviations to the breakdown of perturbation theory in a region where the coupling constant f is of order unity.

Measurements of λ at higher pressures have only been made in cell D, and over a limited temperature range (see Fig. 2). Results of model E_s fits to these data are given in entries 8–10 in parts a and b of Table V. The fits are quite satisfactory over this limited range, but at the highest pressure one suspects that an improvement might be possible.

Generally speaking, the minimum σ [Eq. (4.11)] to be expected is of order $\bar{R}_\lambda \Delta_s$, where $\bar{R}_\lambda$ is an average value of $\hat{R}_\lambda$, and Δ_s is the root-mean-square scatter of the experimental points. Since $\bar{R}_\lambda \approx 0.3$ we expect a minimum σ in the range 3×10^{-4} to 10^{-3} for a scatter of 0.1 to 0.3%. It is therefore clear that none of the fits discussed so far have attained this limit, except perhaps those at $P = 6.9$ and 14.7 bars, for which data only exist over a narrow temperature range. Moreover, if we examine the values of $f(t)$ obtained in the fits, we see that in most cases the bulk of the data are in regions where f is of order unity, so the truncation of Eqs. (3.16) and (3.17) is not expected to be an accurate approximation. It is therefore useful to study the effect of this truncation numerically, as we do in Sec. IV B 4.

TABLE VI. Fit of thermal conductivity to experiment as in Table V, except that model F is used, with a singular C_P and the effective exponent ν, Eq. (3.12), nonzero.

Fit	Cell	Range	t_0	B_3	w_0'	f_0	w_0''	$10^3\sigma$
			(a) $c_d = c_4 = 0.25$					
1	A	$0.003 < t < 0.01$	10^{-2}	0[a]	0.396	0.510	−0.168	1.0
2	A	$t < 10^{-2}$	10^{-2}	0[a]	0.332	0.620	+0.415	8.1
3	A	$t < 10^{-2}$	10^{-2}	0.225	0.314	0.608	−0.355	1.0
4	D 0.0	$t < 10^{-2}$	10^{-2}	0[a]	0.294	0.666	+0.192	5.8
5	D 0.0	$t < 10^{-2}$	10^{-2}	0.139	0.306	0.612	−0.149	1.3
6	D 6.9	$t < 3\times10^{-4}$	10^{-2}	0.139[a]	0.378	0.371	−0.199	1.0
7	D 14.7	$t < 3\times10^{-4}$	10^{-2}	0.139[a]	0.327	0.379	−0.050	1.1
8	D 22.3	$t < 5\times10^{-4}$	10^{-2}	0.139[a]	0.354	0.237	−0.056	0.6
			(b) $c_d = c_3 = 0.107$					
1	A	$0.003 < t < 0.01$	10^{-2}	0[a]	0.595	0.407	−0.170	1.0
2	A	$t < 10^{-2}$	10^{-2}	0[a]	0.400	0.634	+1.360	9.1
3	A	$t < 10^{-2}$	10^{-2}	0.220	0.567	0.424	−0.568	1.2
4	D 0.0	$t < 10^{-2}$	10^{-2}	0[a]	0.348	0.713	0.717	8.0
5	D 0.0	$t < 10^{-2}$	10^{-2}	0.173	0.480	0.487	−0.307	1.2
6	D 6.9	$t < 3\times10^{-4}$	10^{-2}	0.173[a]	0.622	0.269	−0.384	0.9
7	D 14.7	$t < 3\times10^{-4}$	10^{-2}	0.173[a]	0.559	0.233	−0.179	1.1
8	D 22.3	$t < 5\times10^{-4}$	10^{-2}	0.173[a]	0.637	0.133	−0.248	0.5
9	A	$t < 10^{-2}$	10^{-2}	0.224	0.595[a]	0.407[a]	−0.785	2.5
10	A	$t < 10^{-2}$	1	0.224	0.481[a]	0.0208[a]	−0.368	2.2

[a]Parameter held constant in the fit.

TABLE VII. Fit of thermal conductivity to experiment, using model E as in Table V, except that model E_0 is used in fits 5 and 6 (i.e., the singular C_P is replaced by the constant C_{Pb}). The initial value w_0'' of the imaginary part of the ratio w and the parameter $\epsilon = 4 - d$ are also varied in a number of the fits.

Fit	Cell	C_P	Range	t_0	c_d	B_3	w_0'	f_0	w_0''	$10^3\sigma$
1[a]	D 0.0	C_{Ps}	$t < 10^{-3}$	10^{-3}	0.25	0[b]	0.482	0.844	0[b]	1.3
2	A	C_{Ps}	$t < 10^{-2}$	10^{-2}	0.107	0[b]	1.165	0.235	−1.406	6.0
3	A	C_{Ps}	$t < 10^{-2}$	10^{-2}	0.107	0.186	1.159	0.236	3.574	4.8
4	D 0.0	C_{Ps}	$t < 10^{-2}$	10^{-2}	0.107	0.132	0.966	0.273	−3.000	3.0
5	A	C_{Pb}[c]	$0.003 < t < 0.01$	10^{-2}	0.107	0[b]	0.329	0.427	0[b]	1.8
6	A	C_{Pb}[c]	$t < 10^{-2}$	10^{-2}	0.107	−0.233	0.371	0.378	−1.340	1.8
7[d]	D 0.0	C_{Ps}	$t < 10^{-3}$	10^{-3}	0.25	0[b]	0.465	0.856	0[b]	1.7

[a]ϵ in Eq. (3.16) adjusted, yielding $\epsilon = 1.02$.
[b]Parameter held constant in the fit.
[c]$C_{Pb} = 9.792$ J mole^{-1} K^{-1}.
[d]ϵ in Eq. (3.16) fixed at $\epsilon = 1.06$.

4. *Phenomenological three-loop term*

We solve the recursion relations numerically with the term $B_3 wf^3$ added to the right-hand side of Eq. (3.17) as in Sec. III B, and treat B_3 as a further adjustable parameter in the fits. The results of this procedure for model F are shown in Fig. 18(a) (solid lines) for the vapor-pressure data in both cells A and D. The corresponding quantitative information is given in entries 3 and 5 in parts a and b of Table VI (for the 2 values of c_d). The addition of the parameter B_3 improves the fits to essentially their lower limit, and yields coefficients B_3 of order 0.2, i.e., values which are consistent with theoretical expectations (a number much higher than unity would be unphysical). The results in the tables show that the three-loop term affects the initial values w_0 and f_0 only moderately so that setting $B_3=0$ in the finite $-B_3$ fit does not destroy the agreement in the weak-coupling range $t \gtrsim 10^{-3}$ [see dashed line in Fig. 18(a)].

The values of B_3 obtained in cells D and A for the two values of c_d are of order 0.14–0.23 (see 3 and 5 in parts a and b of Table VI) which leads to $w^* \approx 0.15 \sim 0.27$ in three dimensions, and $d^* \approx 2.6$ (see Fig. 6). The leading correction exponent x_1 can also be calculated, and it is in the range $0.08 \lesssim x_1/\nu \lesssim 0.13$. As mentioned previously,[60] we do not consider our estimate of d^* to be totally reliable, but our analysis shows that the value $d^* \approx 3$ obtained by neglecting higher-loop terms,[18,24,25] is even less trustworthy.

We can once again demonstrate that the improved fit obtained in model F is not merely due to the additional parameter, by repeating the above procedure using model E_s (see entries 3 and 5 in parts a and b of Table V and entry 3 of Table VII). In this case the quality of the fit only improves slightly with adjustment of B_3 or w_0'', so we conclude that the specific-heat variation is the crucial element in the success of model F. According to the theoretical analysis of Sec. III C we know that this is the case at sufficiently high temperatures (see Fig. 8) and the fit

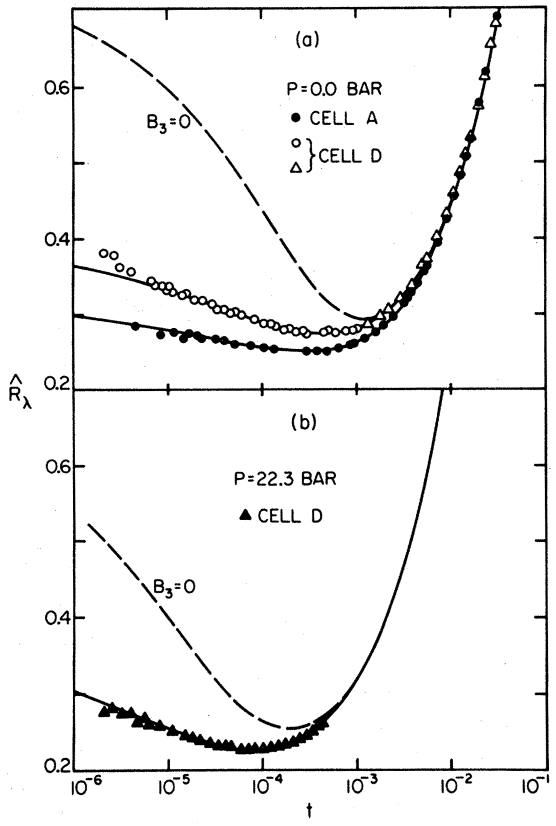

FIG. 18. (a) Fits of the data in cells A and D at $P=0$ to model F including f_0, w_0' and w_0'', as well as the coefficient B_3 of the phenomenological three-loop term as adjustable parameters (solid lines). The dashed line is calculated by setting $B_3=0$ in the equations, but retaining the initial values obtained in the fit to cell A with $B_3 \neq 0$. The fits are listed in entries 3 and 5 in part b of Table VI. The open triangles are data generated by the procedure discussed in Sec. II D. (b) Model F fit to the data in cell D at $P=22.3$ bars, with B_3 fixed at its value obtained for cell D in part (a), and the initial values f_0, w_0', and w_0'' adjusted. The dashed line is calculated by setting $B_3=0$ as in part (a). The parameters of the fit are given in entry 8 in part b of Table VI.

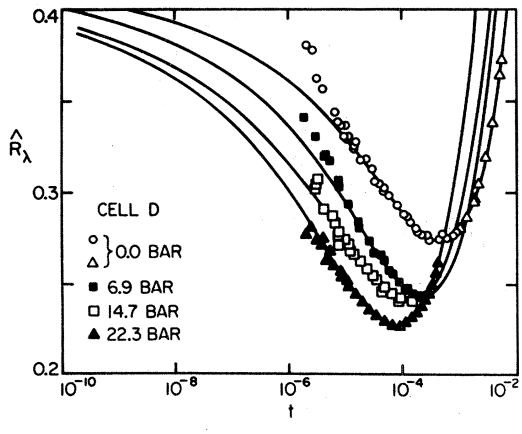

FIG. 19. Model F fits to the data in cell D at various pressures. The adjustable parameters are the initial values f_0, w_0', and w_0''; the coefficient of the three-loop term has been fixed at its values $B_3=0.173$ obtained at $P=0$. The values of the parameters are listed in entries 5–8 in part a of Table VI.

demonstrates the importance of a consistent treatment of C_P everywhere. Indeed, we have also carried out a fit with a *constant* C_P (model E_0), and find better agreement than in model E_s, but worse than in model F (see fits VII.5, 6). Another interesting test is to fix w_0 and f_0 at their values obtained in the limited-range fit 1 in part b of Table VI, and to adjust w_0' and B_3 using all the data, which results in a fit with σ intermediate between models E_s and F (see entry 9 in part b of Table VI).

Having determined the contribution of three-loop and higher terms phenomenologically from measurements at vapor pressure, we now wish to analyze the higher-pressure data, assuming B_3 to be universal.[61] The results using model F are shown in entries 6–8 in parts a and b of Table VI and in Figs. 18(b) and 19. The quality of the fit is excellent in all cases, thus verifying the consistency of our procedure. Moreover, for $P=22.3$ bars (entry 8 in parts a and b of Table VI) the improvement over model E_s (entry 10 in parts a and b of Table V) is nonnegligible even though no additional adjustable parameter is used (B_3 is fixed from elsewhere, and w_0' can be shown not to improve the fit by itself, cf. 2 in Table VII and in part b of Table V). Figures 18(b) and 19 show the quality of the fit as well as the very slow approach to a universal R_λ predicted by the present analysis.

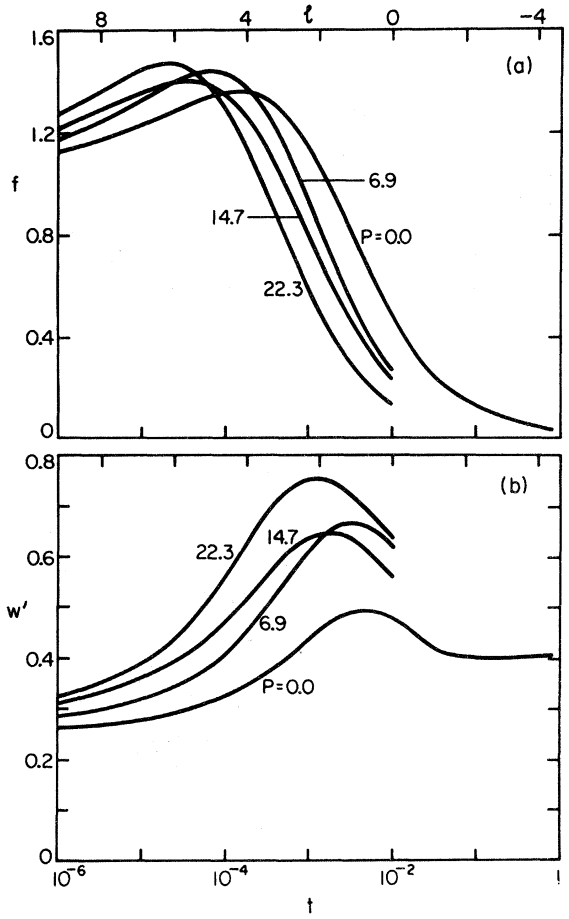

FIG. 20. Functions $f(t)$ and $w'(t)$ resulting from the model F fits listed in entries 5–8 in part b of Table VI. When inserted into Eqs. (3.13) and (3.28), with $c_d=0.107$, these functions give an excellent fit to the data in cell D. Values of l are given on the top scale.

It is interesting to compare the $B_3=0$ curve at vapor pressure [Fig. 18(a)] with the corresponding one at $P=22.3$ bars [Fig. 18(b)]. At the higher pressure, the $B_3=0$ curve agrees with the $B_3\neq 0$ curve over a larger temperature range than at vapor pressure. This is because the bare coupling constant is smaller at high pressures (see Table I) so the effect of three-loop terms comes in closer to T_λ.

In Fig. 20 we show the functions $f(l)$ and $w'(l)$ obtained by our model F fits at the different pressures. When inserted into Eq. (3.28), these functions yield an excellent representation of the thermal conductivity data over the temperature range $10^{-6}<t<10^{-2}$. In order to facilitate use of these functions for other purposes (e.g., to calculate second-sound damping or light scattering), we have tabulated them for both $c_d=c_4=0.25$ and $c_d=c_3=0.107$ and published the numerical values elsewhere.[62]

C. Behavior at high temperatures

In Sec. IV B the thermal conductivity was discussed in the range $10^{-6}<t<10^{-2}$, and we now wish to consider the high-temperature region $10^{-2}<t<1$. The designation of this region as "high-temperature" is appropriate because it corresponds to $t>t_c$, where $t_c\approx 10^{-3}$ is the crossover temperature. Figure 15 shows the experimental thermal conductivity in cell A, as well as the high-temperature data of Kerrisk and Keller,[33] along with our best model F fit (entry 3 in part b of Table VI). As expected, the agreement with model F is good out to $t=10^{-2}$, and it continues to be good until $t\approx 5\times 10^{-2}$, but the theoretical curve is flat for higher t, whereas the data have a smooth rise, coming from regular transients. The explanation for this dependence might be sought in the variation of the mode-coupling parameter g_b in Eq. (2.2). Indeed, let us replace this constant by

$$g_b(T)=\frac{\sigma(T)k_BT}{\hbar}\ , \tag{4.12}$$

where $\sigma(T)$ is the experimental entropy, listed in

Table III. Then the model F fit is only slightly changed for $t < 10^{-2}$, whereas the predictions for $t > 10^{-2}$ are very different with a variable coupling constant (dotted curve in Fig. 15). Although the agreement is no better than for a constant g_b, the calculation shows that regular transients are an important effect for $t > 10^{-2}$, and that the model with constant bare parameters g_b, λ_b, Γ_b cannot be expected to apply in this region.

We therefore wish to consider a model with bare parameters which are specified but unknown *analytic* functions of the absolute temperature, $g_b(T)$, $\lambda_b(T)$ and $\Gamma_b(T)$, and to carry out the renormalization-group procedure on this more general model, which we shall call model $F(T)$. [The static parameters will for the moment be assumed to be known (including all transients), either from experiment or theory.] A complete formulation of the renormalization group for model $F(T)$ seems to be rather difficult, but we can use the high-temperature expansion of model F discussed in Sec. III C to find an accurate approximation to λ in the region where $F(T)$ differs from F ($t > 10^{-2}$) and neglect the difference closer in.

Specifically, we take Eq. (3.46) for the thermal conductivity in model F

$$\lambda(\kappa) = \lambda_\infty \left[1 + \frac{\tilde{f}_\infty \pi}{8\kappa} [1 + \tilde{\lambda}_2(\kappa)] \right] , \tag{4.13}$$

where $\tilde{f} \equiv f\kappa$, and identify λ_∞ and $\tilde{f}_\infty$ in model F as λ_b and $\tilde{f}_b$, as mentioned in Sec. II A. This means that for model $F(T)$ we may write

$$\lambda(T, \kappa) = \lambda_\infty(T) \left[1 + \frac{\pi \tilde{f}_\infty(T)}{8\kappa} [1 + \tilde{\lambda}_2(\kappa)] \right] , \tag{4.14}$$

where we neglect the regular T dependence of the correction $\tilde{\lambda}_2(\kappa)$, since this term only contributes significantly close to T_λ. The notation in Eq. (4.14) is intended to separate the regular temperature dependence (denoted by T) from the singular dependence which occurs via κ. Equation (4.14) forms the basis for a fit to experimental data over the whole temperature range $t < 1$, treating the analytic functions $\lambda_\infty(T)$ and $\tilde{f}_\infty(T)$ as adjustable. We shall summarize the main steps of this analysis here, and give the details in Appendix C. The basic idea consists in choosing a matching temperature t_m (we pick $t_m = 10^{-2}$), where the high-temperature expansion (3.41) is valid, but where the regular T dependence is no longer important. In the region $t > t_m$ we carry out a fit of the data to model $F(T)$ via (4.14) with as many adjustable parameters as necessary.[63] For $t \leq t_m$ models F and $F(T)$ are assumed to have identical behavior, so one can use the model $F(T)$ calculation at $t = t_m$ to obtain *initial conditions* for model F. In this way one obtains a *prediction for the thermal conductivity in the critical range* $t < 10^{-2}$ *using only data outside this range.* The results are shown by the solid curve in Fig. 21, which agrees with the data in the whole weak-coupling region. The deviations for $t < 5 \times 10^{-4}$ are presumably explained by truncation errors in the theory, as discussed above. Indeed, if we fix w_0 and f_0 at $t = 10^{-2}$ at their values determined from the high-t fit, we may then introduce the three-loop term B_3 as before, and adjust it (as well as w_0'') to obtain the fit given by the dashed line. The actual procedure we use is somewhat more involved than described here, and it is discussed in more detail in Appendix C.

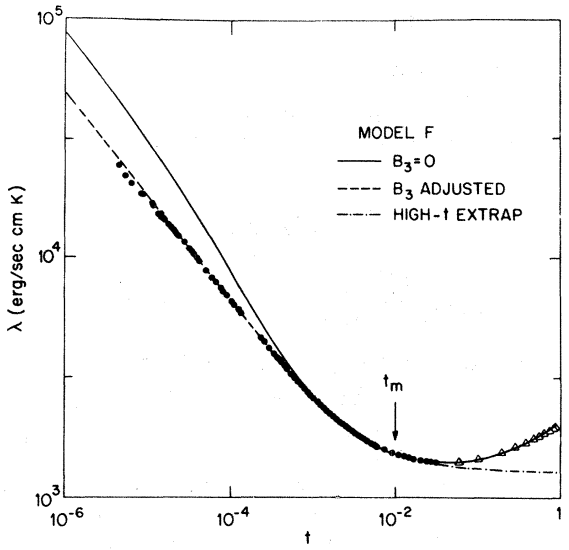

FIG. 21. Thermal conductivity vs reduced temperature on log-log scales, as in Fig. 15. The solid line through the triangles for $t > t_m$ is the high-temperature fit [Eqs. (C1)–(C4)]. The solid line for $t < t_m$ is a model F prediction using parameters obtained from analysis of data for $t \geq t_m$ only. The dot-dashed line for $t > t_m$ is the extrapolation to high temperatures of this model F prediction. The dashed line is a modification of the model F prediction obtained by adjusting the three-loop coefficient B_3 and the initial value w_{01}'' (fit 10 in part b of Table VI).

D. Second-sound damping

As was noted by Dohm and Folk[24] and subsequently by Ferrell and Bhattacharjee,[32] the determination of the background values λ_b and Γ_b permits a calculation of the second-sound damping below T_λ without adjustable parameters. We have done this with our parameter values, using the model E formula derived by Dohm and Folk[24] for the damping con-

stant of second sound

$$D_2 = 2\hat{R}_2 c_2 \xi_T \ . \tag{4.15}$$

In (4.15) c_2 is the second-sound velocity,[36] $\xi_T = \xi_T^0 t^{-\nu}$ is the transverse correlation length with[40]

$$\xi_T^0 = 3.57 \times 10^{-8} \text{ cm} \ , \tag{4.16}$$

and the amplitude ratio is given by[24]

$$\hat{R}_2 = \left(\frac{\xi_L^0}{\xi_T^0}\right)\left(\frac{2u^*(1-2u^*)}{w'(l)f(l)}\right)^{1/2} \phi(w(l),f(l)) \ , \tag{4.17}$$

with ϕ defined[64] in Eq. (19) of Ref. 28, $\xi_L^0/\xi_T^0 = 0.33$, and l now related to the reduced temperature by

$$-2t = t_0 e^{-l/\nu} \ . \tag{4.18}$$

If we fix u^* at its second-order value $u^* = 0.04$ used in (3.25), we may calculate $\hat{R}_2$ from (4.17), with the functions $w'(l)$ and $f(l)$ obtained in the fits to the thermal conductivity above the transition.[62]

The results for our best-fit functions at vapor pressure (entries 3 and 5 in part a of Table VI with $c_d = 0.25$) are shown in Fig. 22(a) and yield excellent agreement with the data of Ahlers,[29] Hanson and Pellam,[65] and the more recent higher-precision data of Robinson and Crooks.[31] The corresponding values of D_2, Eq. (4.15), are shown in Fig. 22(b) where the rise away from T_λ is seen to be correctly reproduced. The result of Dohm and Folk[28] obtained by the same procedure but with different parameters [Fig. 7 of Ref. 25, dot-dashed lines in Figs. 22(a) and 22(b)] is somewhat less accurate, especially away from T_λ. Ferrell and Bhattacharjee[32] obtained a slightly steeper D_2, which goes below the Dohm and Folk prediction and below the data for $|t| > 10^{-3}$.

We may also use the finite-pressure fits in cell D (Table VI part a fits 6–8), to predict the pressure variation of the damping, as shown in Figs. 23(a) and 23(b). The pressure dependence at $t = -10^{-3}$ is shown in Fig. 24, together with values extracted from light scattering data.[30] The agreement between experiment and theory is quite good, except[32] at $P = 2$ bars, where the light scattering intensity is weak and systematic errors might be expected. The prediction of Ferrell and Bhattacharjee,[32] that the precritical rise in D_2 is smaller at high pressure than at vapor pressure, is reflected in the variation in Fig. 23(b) for $|t| < 3 \times 10^{-4}$. For larger $|t|$ the background dominates and D_2 increases with increasing pressure.

It should be noted that the excellent agreement we obtain in Fig. 22 depends crucially on using the fixed-point value $u^* = 0.04$ (obtained from the ϵ expansion in second order) in (4.17). Indeed, if we replaced u^* in (4.17) by

$$u = g_b^2 k_B (-2t)^\nu / 16\pi^2 \xi_0 C_P^- c_2^2 \ , \tag{4.19}$$

as implied in Eq. (A15) of Dohm and Folk,[28] we would reduce $\hat{R}_2$ by roughly 0.06 (independent of t),

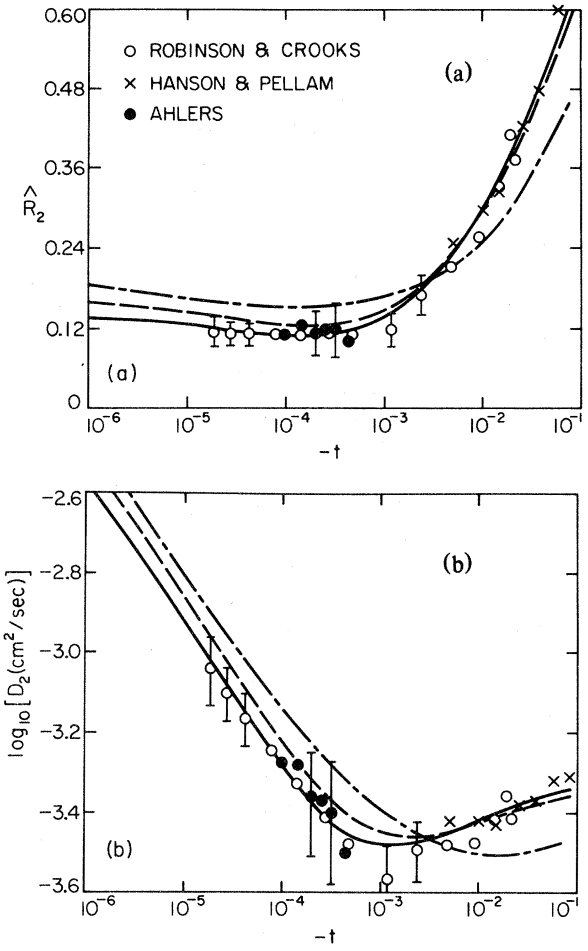

FIG. 22. (a) Comparison of theoretical values of the effective amplitude $\hat{R}_2$, Eq. (4.17), of second-sound damping at saturated vapor pressure with experimental data. Solid line: based on $f(l)$ and $w'(l)$ obtained from a model F fit to λ in cell A (fit 3 in part a of Table VI). Dashed line: based on $f(l)$ and $w'(l)$ obtained from a model F fit to λ in cell D (fit 5 in part a of Table VI). Dot-dashed line: based on $f(l)$ and $w'(l)$ obtained from a model E_s fit by Dohn and Folk and given in Fig. 7 of Ref. 25. Open circles: data from Ref. 31. Crosses: data from Ref. 65 (see also Ref. 29 for the conversion of the measured second-sound attenuation to D_2). Solid circles: data from Ref. 29. Representative error bars for data from Refs. 29 and 31 are shown only on a few points to avoid crowding the figure. (b) The second-sound damping D_2, Eq. (4.15), corresponding to the values of $\hat{R}_2$ shown in (a).

thus reducing the critical value R_2 by almost a factor of 2. Another possibility is to define $\hat{R}_2$ from Eq. (4.15), and to calculate D_2 from Eq. (18) of Ref. 28, which leads to

$$\hat{R}_2 = \left(\frac{g_b^2 \xi_0 C_P^+}{2\pi^2(-2t)^\nu (C_P^-)^2}\right)^{1/2} \frac{\phi(f(l),w(l))}{2c_2\xi_T[w'(l)f(l)]^{1/2}} \ . \tag{4.20}$$

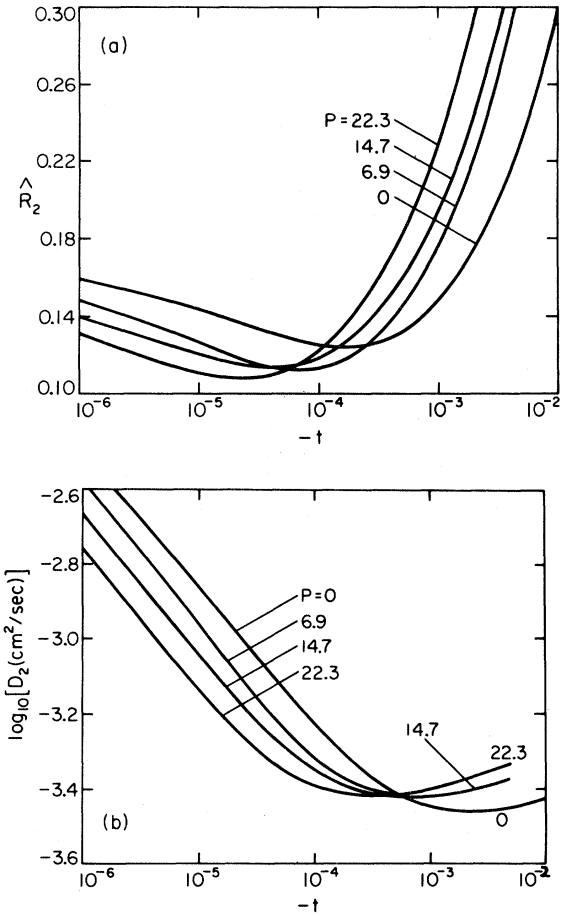

FIG. 23. (a) Effective amplitude $\hat{R}_2$ calculated from functions $f(l)$ and $w'(l)$ obtained from model F fits to the thermal conductivity of cell D above T_λ at several pressures (fits 5–8 in part a of Table VI). The numbers in the figure are the pressure in bar. (b) The second-sound damping D_2 corresponding to the values of R_2 shown in (a).

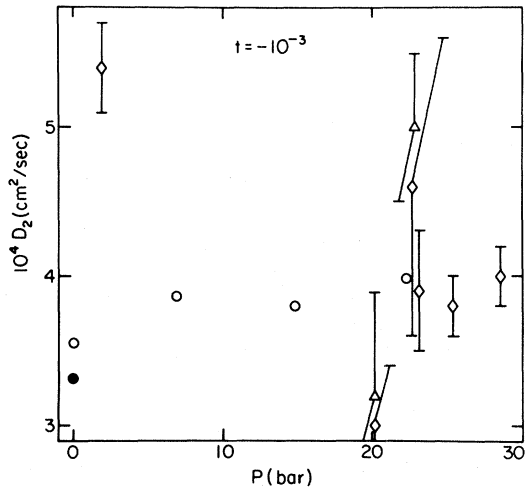

FIG. 24. Second-sound damping D_2 as a function of pressure at a reduced temperature $t=-10^{-3}$. Open circles: based on $f(l)$ and $w'(l)$ obtained from the model F fits to λ in cell D (fits 5–8 in part a of Table VI). Solid circle: based on $f(l)$ and $w'(l)$ obtained from model F fit to λ in cell A (fit 3 in part a of Table VI). Open diamonds are from Tarvin *et al.*, Ref. 30(b) [error bars given by Greytak, Ref. 30(a)]. Open triangles are from Vinen and Hurd, Ref. 30(c) (error bars are approximate and were not given by the original authors).

Use of (4.20) causes a further reduction of $\hat{R}_2$, by about 0.03. These various choices of u correspond to different ways of extrapolating the *static* ϵ expansion to three dimensions, and could presumably be made consistent among one another by a more accurate static theory.

Another point to remember is that we are using a model E_0 formula[28] for $\hat{R}_2$ with model F parameters. We therefore do not know precisely how to insert the proper factors of the singular specific heat, or the $O(v)$ corrections to the function ϕ. (Above T_λ we have done the former correctly, but not the latter.) Pending resolution of the various experimental and theoretical ambiguities, we can say that the second-sound damping appears to be well described by the theory.

V. DISCUSSION AND CONCLUSION

A. Comparison with earlier work

As mentioned in the Introduction, Ferrell and Bhattacharjee[19–21] correctly identified various features of the critical dynamics of ^{4}He, such as the effect of a small w^* on the amplitude of slow transients near the fixed point, and the existence of a high-temperature perturbation theory in κ^{-1}. Their quantitative evaluation of these effects, however, and their explanation of the small t_c, are incomplete so that the precise agreement they found between their theory and experiment depends on unphysical choices for the parameters. Indeed, as regards the smallness of t_c, Eq. (2) of Ref. 19,

$$\kappa_c=(a/B_s)^2 \ , \tag{5.1}$$

can be transcribed into our notation as

$$\kappa_c=t_c^\nu=(K_d g_b^2 \xi_0/f^* C_P)/(\lambda_b/C_{Pb})^2$$
$$=(\tilde{f}_b/f^*)(C_P/C_{Pb})w_b \ . \tag{5.2a}$$

This relation was obtained[19] by equating the critical part $ak^{3/2}$ of the characteristic frequency, to its background value[66] $B_s k^2$. The smallness of t_c was then asserted to come from the critical behavior of the specific heat in the denominator of (5.2a) and from the large value of λ_b. The discussion in Sec. III, however, demonstrates that the critical region is

determined by

$$t_c^{\nu} = \kappa_c = (\pi/8)(K_d g_b^2 \xi_0/\lambda_b \Gamma_b) = (\pi/8)\tilde{f}_b \ , \qquad (5.2b)$$

rather than by (5.2a). In particular the critical specific heat has essentially nothing to do with t_c, since similar values of t_c were found in Fig. 10(a) for model E_0 (with constant C_P) and in Fig. 13 for model F with singular C_P. Finally, Eq. (5.2a) is contradicted by the results in Fig. 11(a) where t_c is shown to be insensitive to the value of λ_b or w_b at *fixed* $\tilde{f}_b$ (we assume $\lambda_{01} = \lambda_b$, $w_{01} = w_b$, $f_{01} = \tilde{f}_b$).

Another restriction on the critical region was asserted[19,67] to come from the small value of w^*. In fact, Fig. 12 above shows that w^* determines the effective exponent of λ for $t < t_c$, but does not influence the value of t_c. Ferrell and Bhattacharjee[19] calculated the effect of w^* on the asymptotic behavior of the thermal conductivity by using the "linear" approximation in Eq. (4.2) above. As discussed by Dohm and Folk[25] and by us in Sec. IV A, this approximation is not valid in the temperature range of the data, so the relatively good fit found in Ref. 19 and in Fig. 14(b) above cannot be considered evidence in favor of a small w^*.

In the high-temperature domain, Ferrell and Bhattacharjee have used a quite separate formalism[20,21,55] to calculate the small departures of the thermal conductivity from its background value via perturbation theory in κ^{-1}. In Eq. (B25) of Appendix B, we show that the high-temperature result of Ref. 55 is, in our notation

$$\lambda = \lambda_\infty \left\{ 1 + \frac{\tilde{f}_\infty \pi}{8\kappa} \left[1 - \frac{a_2}{\kappa} + O\left(\left[\frac{a_2}{\kappa} \right]^2 \right) \right] \right\} \ , \qquad (5.3)$$

where

$$a_2 = 0.145 \tilde{f}_\infty C_{P\infty} / w'_\infty C_P \ . \qquad (5.4)$$

The term in κ^{-1} agrees precisely with our result (3.41) and (3.44) (for both model E_0 and model F), and the next term corresponds to

$$\tilde{\lambda}_2 = -5.88 \times 10^{-3} \kappa^{-1} \ ,$$

for model E_0, with $C_P = C_{P\infty}$, $\tilde{f}_\infty = 0.020$, and $w'_\infty = 0.493$, as depicted by the dot-dashed line in Fig. 9. The difference between our model E_0 result for $\tilde{\lambda}_2$ (dashed line) lies presumably in the fact that $\tilde{\lambda}_2$ was calculated exactly to leading order in Ref. 55, whereas our evaluation does not contain all second-order terms, since the f^2 correction is missing in (3.26).

Ferrell and Bhattacharjee,[16,55] in fact, consider not model E_0 but a simplified version of model F in which the specific heat is taken from experiment, but its effective exponent $\alpha_e = 4\nu/\nu$ is neglected. Although this model is analogous to our model E_s, it has the advantage of giving the right leading correction in (5.3) (i.e., C_P correctly drops out). The term in κ^{-2}, on the other hand [Eq. (5.4)], is multiplied by $C_{p\infty}/C_P$, and thereby reduced in absolute magnitude. Since the treatment of the specific-heat singularity in Ref. 55 is not systematic, the prediction for the κ^{-2} correction cannot be considered reliable, except in order of magnitude.

In applying the high-temperature theory to the experimental data, it is essential to note that the expansion is not in κ^{-1} but in (κ_c/κ), with $\kappa_c = (\pi/8)\tilde{f}_b \ll 1$. Ferrell and Bhattacharjee observed[20] that this variation is consistent with the experimental data, but they gave no theoretical argument to support it. Moreover, they applied the expansion in the region $200 < \kappa^{-1} < 800$, which is well beyond the range $\kappa^{-1} \lesssim 20$ where one or two terms suffice (see Fig. 9). We may estimate the accuracy of the procedure of Ferrell and Bhattacharjee,[20,55] by comparing the value of λ_∞ we obtain from a fit at vapor pressure to Eq. (2.9) for $t > 4 \times 10^{-5}$ ($\lambda_\infty = 1472$ erg/sec cm K, fit 1 of Table II) on the one hand, to the value we find in Appendix C using Eq. (4.13) for $t > 10^{-2}$ ($\lambda_\infty = 1267$ erg/sec cm K, fit 4 of Table VIII) on the other hand.

TABLE VIII. Fit of thermal conductivity in cell A to Eqs. (C1)–(C4) of the text, in the range $t > t_m$, with $\tilde{\lambda}_2(\kappa) \equiv 0$.

Fit	$\lambda_{\infty 0}$	$\lambda_{\infty 1}$ (erg/cm sec K)	$\lambda_{\infty 2}$	$10^2 f_{\infty 0}$	$f_{\infty 1}$	σ	t_m
1	1268 ±9	839 ±22	0[a]	2.4 ±05	0[a]	32	10^{-3}
2	1382 ±25	691 ±39	0[a]	0.7 ±0.4	0[a]	34	10^{-2}
3	1236 ±3	1385 ±23	−680 ±28	2.6 ±02	0[a]	9	10^{-3}
4	1267 ±12	1286 ±46	−600 ±45	2.1 ±2	0[a]	10.5	10^{-2}
5	923 ±28	199 ±50	−103 ±27	5.0 ±0.3	2.4 ±3	3.9	10^{-2}
6	1235 ±5	1389 ±30	−684 ±34	2.6 ±0.04	0[a]	10	3×10^{-3}

[a]Parameters held constant in the fit.

This comparison shows that the neglect of regular transients and the use of the expansion beyond its range of validity lead to errors of 15–20% in the value of λ_∞.[68] The terms in κ^{-1} also differ by the same amount in the two fits, leading (coincidentally) to agreement for the ratio $\lambda_1 = 8 \times 10^{-3}$. In Ref. 55 an approximate evaluation of the higher terms [Eq. (4.2) of Ref. 55], was used to extract the values $\lambda_b = 1300$ erg/sec cm K and $\Gamma_b = B_\psi = 1.1 \times 10^{-4}$ cm^2/sec, at $P = 22.3$ bars, corresponding to $\lambda_1 \approx 5.7 \times 10^{-3}$. It is not clear, however, how accurate this value is, since it results from an uncontrolled approximation to $\tilde{\lambda}_2(\kappa)$ [Eq. (3.46)], which neglects the effects of the important quantity v, Eq. (3.12).

Turning now to the paper by Hohenberg, Halperin, and Nelson,[18] we have already discussed the inadequacy of the quadratic approximation for a quantitative fit over the whole temperature range. This point was first made by Dohm and Folk,[25] who compared various power-law truncations to an exact integration of the model E equations. It should be noted, however, that the quadratic approximation was shown[25] to be quite accurate for $t < 10^{-3}$, and it only failed for higher temperatures. Moveover, the reason for this failure lies in the small value of the initial coupling f_{01}, rather than in the fixed-point value w^* as implied in Ref. 25.[69] The quadratic approximation is thus adequate to treat the problem of a small w^* (as claimed in Ref. 18), but it fails for $t \gtrsim t_c$, wherever this crossover may be.

Independently of Ref. 18, Dohm and Folk[24,25] carried out an analysis of the thermal conductivity using the full nonlinear equations, and a fitting of initial values analogous to the procedure we employ. Although the point of view and general methodology of Dohm and Folk are similar to ours, the quantitative results differ, and we can only agree with their semiquantitative conclusions. These are that the full nonlinear renormalization group is necessary to describe the thermal conductivity over the whole temperature range $10^{-6} < t < 1$, that f decreases away from T_λ, and that the result $w^* \ll 1$ inferred from the ϵ expansion,[13–18] is consistent with experiment. The quantitative claim of Dohm and Folk[24,25] that the data can only be fitted for $|3 - d^*| < 0.1$ (i.e., $w^* \approx 0$) is, in our opinion, unreliable for the following reasons:

(i) The initial values f_0 and w_0 at $t_0 = 10^{-3}$ were adjusted to fit data in the range $10^{-6} < t < 10^{-3}$, for various values of $d - d^*$, and the best fit was obtained for $|d - d^*| \lesssim 0.1$. The difficulty with this procedure is that the theory is most sensitive to truncation errors in this temperature range, since f is of order unity there. In fact, the best fit of Dohm and Folk in this range deviates significantly from the data when extended to $t > 10^{-3}$ (see the solid line in Fig. 17).

If data out to $t = 10^{-2}$ are included in a model E_s fit, one finds that the overall quality of the fit deteriorates (see fits 2 and 4 in parts a and b of Table V). Treating d^* as an adjustable parameter does not improve the fit significantly in model E_s, and d^* remains near 3 (see fits 3 and 5 in parts a and b of Table V).

(ii) In practice, f_0 and w_0 at $t_0 = 10^{-3}$, say, are more reliably determined from data in the weak-coupling regime $t > 10^{-3}$. To do this, however, one needs an accurate weak-coupling theory, and this necessitates use of model F and not model E_s.

(iii) A problem with the analysis of Dohm and Folk[25] is that the adjustment of d^* was made by adding constant (f-independent) terms to the curly brackets in Eqs. (3.16) and (3.17) above. This effectively changes the value[70] of ϵ, to $\tilde{\epsilon}$, say, in Eq. (3.16), whereas ϵ was kept equal to 1 in calculating λ from (3.13). Thus λ had a spurious dependence on $\kappa^{(\tilde{\epsilon}-\epsilon)/2}$ for $t \gg t_c$, which would affect the accuracy of the calculation in the weak-coupling regime, even with model F. The procedure we use to adjust d^* involves an f-dependent term (3.34) which becomes negligible for $t \gtrsim t_c$.

Thus, although Dohm and Folk correctly emphasized the importance of the high-temperature limit, the anlaysis they carried out is inaccurate in the range $t \gtrsim t_c$ where the theory is in principle systematic.[71]

B. Conclusion

We conclude by first stating the principal results of the present investigation:

(i) The critical dynamics of ^{4}He is characterized by a crossover from a weak-coupling regime at high reduced temperatures $t_c \ll t \ll 1$, to a scaling regime near T_λ ($t \ll t_c$) with $t_c \approx 10^{-3}$. The smallness of the crossover temperature t_c comes about because the bare dynamic coupling constant is anomalously small ($f_b \approx 0.02$), and not because of a large background λ_b or a small ratio w^* (Figs. 10–12).

(ii) The dynamic renormalization group based on model F of Halperin *et al.*[11] can be meaningfully tested in the crossover region $10^{-3} < t < 10^{-2}$, using parameters extracted from an analysis in the range $t > 10^{-2}$ and from static experiments. The agreement between the nonlinear theory and measurements of the thermal conductivity is excellent in the crossover region (Sec. III C).

(iii) Closer to the transition ($t < 10^{-3}$), the truncation errors associated with perturbation theory[11,13,17,55] in the coupling constant f become nonnegligible, and the theory does not make accurate predictions. Moreover, the experimental situation is at present also unsettled in this region, since different experiments have yielded different results (Sec. II A).

(iv) The theoretical prediction,[13] based on a two-

loop expansion, that the fixed point is close to the weak-scaling instability ($w^*=0$), is roughly consistent with the data, within the 20–30% uncertainties of the theory.

(v) Treating the coefficient of a higher-loop correction as an adjustable parameter, an excellent fit is obtained over the whole range $10^{-6} < t < 1$, with $w^* \approx 0.2$. This means dynamic scaling would only break down for $d < d^* \approx 2.6$ (Sec. IV B 4).

(vi) Model E_0 in which the specific heat is a constant agrees with model F for $t \gtrsim 5 \times 10^{-3}$. The phenomenological model which includes the specific-heat singularity approximately [model E_s (Refs. 11, 18, and 25)] only agrees with model F for $t \lesssim 10^{-5}$ (Fig. 8). The experimental data rule out both models E_0 and E_s, in favor of model F.

(vii) Earlier claims[19,24,25] and suggestions[18] that a quantitative fit can be obtained with model E_s, and that the data prove that $d^* \approx 3$, are not valid.

(viii) The damping of second sound can be calculated and compared with experiment without any adjustable parameters.[24,28] The agreement with most existing data is good, as regards both temperature and pressure dependence. An ambiguity remains, however concerning the absolute magnitude, since different estimates of the *static* parameters below T_λ yield answers which differ by a factor of 2.

Our analysis reveals a number of improvements which can be made in order to provide a more stringent test of the theory.

(i) The experiments should be repeated, and extended to high temperatures over a range of pressures. Clearly the discrepancies revealed in Figs. 3 and 18 between different measurements at vapor pressure must be elucidated.

(ii) The perturbation expansion for model F should be completed to include all terms in f^2 (including v) in Eqs. (3.16), (3.17), and (3.26). If possible, calculations or estimates of the higher-loop contributions should be attempted.

Noted added in proof: Very recently, Dohm and Folk[72] have calculated the missing $O(f^2)$ terms in Eqs. (3.16) and (3.17), though not the ones in (3.26). They have repeated the analysis of the present paper with the new β functions, and have found good agreement with the data without the necessity of introducing a three-loop term. This means that the experiments are consistent with $d^* \approx 3$. Of course, completion of the $O(f^2)$ calculation in Eq. (3.26) or a calculation of higher-loop terms can change the picture, since the value of d^* is determined by data in a temperature region where $f \approx 1$.

(iii) Specific-heat measurements should be extended to higher temperatures and pressures, and analyzed in terms of regular and singular contributions.

(iv) The static renormalization group should be extended to find a quantitative estimate of corrections to the asymptotic power law for κ, and more reliable results below T_λ.

These improvements are all more or less straightforward extensions of what has been done so far, and they would permit a more rigorous test of the theory. It appears to us advisable to analyze high-pressure data first, since the weak-coupling regime extends closest to T_λ in that case [see Fig. 20(a)]. For the study of the asymptotic critical behavior and the determination of w^*, on the other hand, data at vapor pressure appear more promising.

In conclusion we wish to state that in our opinion the considerable labor that has gone into the present analysis and that the next stage would entail, are worth the effort, since this system may be the best candidate for a definitive test of the renormalization-group theory.

ACKNOWLEDGMENTS

The authors are grateful to R. P. Behringer for his aid in the experiments on cell A, and to B. I. Halperin for informative discussions. Thanks are also due to V. Dohm, R. Folk, R. A. Ferrell, J. K. Bhattacharjee, B. J. Robinson, and M. J. Crooks for communicating their results prior to publication. The work of G. A. was partially supported by the NSF under Grant No. DMR-7923-289.

APPENDIX A: TREATMENT OF THE SPECIFIC HEAT AT HIGH TEMPERATURES

As discussed in Sec. II, the experimental specific heat has been fit to a function of the form

$$C_P = (A/\alpha)t^{-\alpha}(1+Dt^{0.5}) + B + Et \ , \tag{A1}$$

with parameters listed in Table I for the pressures of interest. The effective exponent in Eq. (3.12) is given by

$$\alpha_e = 4\nu v = -\frac{d\ln C_P}{d\ln t} \ , \tag{A2}$$

and may easily be calculated from (A1), as shown in Eq. (B14) of Ref. 18. The function $\alpha_e(t)$ is a smooth function in the range $10^{-6} < t < 10^{-2}$, which varies from 0.3 to 0.1, at $P=0$, for instance (see Fig. 7). The function (A1) grows at large t and would lead to a negative α_e at $t = 5 \times 10^{-2}$, as shown by the dashed curve in Fig. 7(a). If instead of (A1) we take the experimental C_P, which has a minimum at $t=0.1$ [Fig. 7(b)], then α_e becomes negative at that point. A correct treatment of the static renormalization group, which separates the regular from the singular transients as we do in Appendix C for the dynamics, would yield a positive α_e everywhere, since the rise of C_P at high temperatures is presumably due to the regular terms (see below). In the present work which

neglects various static transients, we have taken a shortcut in evaluating the high-temperature specific heat; this treatment should be sufficient to obtain a consistent picture of the dynamics in that range, though not a fully quantitative one, for which an accurate theory of static transients is necessary. Our shortcut involves choosing for the effective exponent at high temperatures the function

$$\alpha_e = \alpha_1/t + \alpha_2/t^2 \ , \tag{A3}$$

and matching $\alpha_e(t)$ and $d\alpha_e/dt$ to the equation for α_e obtained from (A1) and (A2) at $t=0.03$, to find $\alpha_1 = 8.07\times10^{-3}$ and $\alpha_2 = -3.73\times10^{-5}$. The function so obtained is shown by the solid line in Fig. 7(a), for $t > 0.03$. Its integral gives the singular specific heat C_P [solid line in Fig. 7(b)] which has the form

$$C_P = C_{P\infty}\exp(\alpha_1/t + \alpha_2/2t^2) \ , \tag{A4}$$

with

$$C_{P\infty} = 9.792 \text{ J/mole K} \ , \tag{A5}$$

obtained by matching at $t=0.03$.

A more systematic analysis, similar to the one we carry out in Appendix C for the dynamics, would fit the specific heat over the whole temperature range to the function

$$C_P = [A(T)/\alpha][\kappa^{-\alpha/\nu}(1+D\kappa^{x_0/\nu})-1]+B(T) \ , \tag{A6}$$

with analytic coefficients

$$A(T) = A_0 + A_1 t + A_2 t^2 + \cdots \ , \tag{A7}$$

$$B(T) = B_0 + B_1 t + B_2 t^2 + \cdots \ . \tag{A8}$$

Then the effective exponent is *defined* by a derivative at constant T,

$$\alpha_e = 4\nu\upsilon = -\nu \left.\frac{d\ln C_P}{d\ln\kappa}\right|_T \ . \tag{A9}$$

This function is expected to remain positive and to vanish at large t, similarly to the solid line in Fig. 7(a), and to Eq. (A3).

APPENDIX B: HIGH-TEMPERATURE EXPANSION: THEORY

Let us first set $\eta^A = 0$ and $\epsilon = 1$ and rewrite Eqs. (3.10), (3.11), and (3.16)–(3.25) (model F) as

$$\frac{\kappa}{f}\frac{df}{d\kappa} = -1 - A_1(w')f + \frac{1}{w'}\mathrm{Re}(w\tilde{h}) + O(f^2) \ , \tag{B1}$$

$$\frac{\kappa}{w}\frac{dw}{d\kappa} = -B_1(w')f - 4\upsilon - \tilde{h} + O(f^2) \ , \tag{B2}$$

$$\frac{\kappa}{C_P}\frac{dC_P}{d\kappa} = -4\upsilon \ . \tag{B3}$$

We now introduce the variables

$$\tilde{f} = f\kappa \ , \tag{B4}$$

$$C_P/C_{P\infty} = \chi \ , \tag{B5}$$

$$\tilde{w} = w/\chi = \tilde{w}' + i\tilde{w}'' \ , \tag{B6}$$

$$\tilde{\lambda} = K_d^{1/2}(\chi/w' f\kappa)^{1/2} = (\tilde{w}'\tilde{f})^{-1/2}K_d^{1/2} \ , \tag{B7}$$

in terms of which Eqs. (B1)–(B3) become

$$\frac{\kappa}{\tilde{f}}\frac{d\tilde{f}}{d\kappa} = -A_1(w')f + \frac{1}{w'}\mathrm{Re}(w\tilde{h}) + O(f^2) \ , \tag{B8}$$

$$\frac{\kappa}{\tilde{w}'}\frac{d\tilde{w}'}{d\kappa} = -B_1(w')f - \frac{1}{w'}\mathrm{Re}(w\tilde{h}) + O(f^2) \ , \tag{B9}$$

$$\frac{\kappa}{\tilde{\lambda}}\frac{d\tilde{\lambda}}{d\kappa} = = -\frac{f}{2} + O(f^2) = -\frac{\tilde{f}}{2\kappa} + O(f^2) \ . \tag{B10}$$

Now according to Appendix A the effective exponent υ decays to zero at large κ on some scale $\kappa_s = O(1)$. The large-κ solutions for Eqs. (B8)–(B10) may then be written in the form

$$\tilde{w}' = \tilde{w}'_\infty[1 + \tilde{w}'_1(\kappa)] \ , \tag{B11}$$

$$\tilde{f} = \tilde{f}_\infty[1 + \tilde{f}_1(\kappa)] \ , \tag{B12}$$

where the functions $\tilde{w}'_1(\kappa)$ and $\tilde{f}_1(\kappa)$ go to zero when $\kappa^{-1}\to 0$. The decay of these functions is on the scale of κ_s, since for small f the dominant term on the right-hand sides of (B1) and (B2) is $\tilde{h}$, which decays as υ. The thermal conductivity is given by

$$\lambda = \lambda_0\tilde{\lambda}(1 - c_d f) \ , \tag{B13}$$

with[39]

$$\lambda_0 = k_B g_b C_{P\infty}^{1/2}\xi_0^{1/2} \ , \tag{B14}$$

so Eqs. (B7) and (B11)–(B14) imply

$$\lambda = \lambda_\infty\{1 + (\lambda_1/\kappa)[1 + \tilde{\lambda}_2(\kappa)]\} \ , \tag{B15}$$

$$\lambda_1 = \tilde{f}_\infty(\tfrac{1}{2} - c_d) = \tfrac{1}{8}\tilde{f}\pi \ , \tag{B16}$$

for $c_d = 0.107$, as in Eq. (3.44) of the text. The function $\tilde{\lambda}_2(\kappa)$ goes to zero, but on the scale κ_s, since $\tilde{w}'_1$ and $\tilde{f}_1$ contribute to this function.

For our numerical illustration we have taken a model F fit to cell A. Specifically, we use $t_0 = 10^{-2}$, $w'_0 = 0.563$, $f_0 = 0.428$, $w''_0 = -0.412$, $B_3 = 0.204$, $c_d = c_3 = 0.107$, and find by integating to $t = 10^3$

$$\begin{aligned} &\tilde{\lambda}_\infty = 2.265, \quad \tilde{f}_\infty = 2.00\times10^{-2} \ , \\ &w'_\infty = 0.493, \quad w''_\infty = -0.220 \ , \\ &C_{P\infty} = 9.79 \text{ J/mole K} \ , \\ &\lambda_0 = 563.0 \text{ erg/cm sec K} \ , \\ &\lambda_\infty = 1275.2 \text{ erg/cm sec K} \end{aligned} \tag{B17}$$

Thus, λ decays to its asymptotic value on the scale $\kappa_c = \frac{1}{8}\tilde{f}_\infty\pi = 0.008$ ($t_c = \kappa_c^{1/\nu} = 7\times10^{-4}$), for *both*

models E_0 and F. The correction $\tilde{\lambda}_2$ shown in Fig. 9 was obtained from an exact integration of the model F equations. It is seen that this function has curvature on the scale $\kappa_s^{-1}=O(1)$ for model F. In model E_0 [obtained by setting $v\equiv 0$ and $\tilde{w}_\infty''=0$ in Eqs. (B1), (B2), and (B6) but keeping the same $\tilde{f}_\infty$ and $\tilde{w}_\infty'$], Fig. 9 shows that $\tilde{\lambda}_2(\kappa)$ varies on the scale κ_c/κ, and only has curvature for $\kappa^{-1}\approx\kappa_c^{-1}=125$.

The model we have treated here, in which $\eta^A=0$, is physically the correct one at large κ since according to Eq. (3.25), η^A depends on the static coupling u which is also expected to decay at large κ (on the scale κ_s). In our fits to the thermal conductivity, however, we have kept the small quantity η^A fixed, and so for consistency in the analysis we must also consider the model for $\eta^A\neq 0$ and constant. For completeness we shall also treat the case $\epsilon\neq 1$ in (B1) [see (3.16)]. The preceding analysis may then be repeated, with the following modifications:

$$\tilde{f}=f\kappa^{\epsilon+\eta^A}\ , \tag{B18}$$

$$\tilde{w}=w/\chi\kappa^{\eta^A}\ , \tag{B19}$$

$$\lambda=\lambda_\infty\left[1+\frac{\lambda_1}{\kappa^{\epsilon+\eta^A}}[1+\tilde{\lambda}_2(\kappa)]\right]\ , \tag{B20}$$

$$\lambda_1=\tilde{f}_\infty\{[2(\epsilon+\eta^A)]^{-1}-c_d\}\ . \tag{B21}$$

Equation (B20) demonstrates that λ must go to a constant at high temperatures for all values of ϵ.

Let us compare the above treatment with that of Ref. 55, in which a coupling constant is defined in Eq. (2.4).

$$g^2\equiv\frac{g_b^2}{C_P\Gamma_\infty\kappa}=\frac{\tilde{f}_\infty}{w_\infty K_d\kappa\chi} \tag{B22}$$

[in rewriting (B22) we have used the fact that $\tilde{f}_\infty=K_d g_b^2/\lambda_\infty\Gamma_\infty$, and $w_\infty=\Gamma_\infty C_{P\infty}/\lambda_\infty$]. Thus Eqs. (2.12), (2.13), (4.2), and (4.3) of Ref. 55 with $b=1$ read

$$\lambda=\lambda_\infty\left[1+\frac{g^2\chi\Gamma_\infty C_{P\infty}}{16\pi\lambda_\infty}[1+a_2' g^2+O(g^4)]\right]\ , \tag{B23}$$

$$a_2'=\frac{8}{15\pi^2}(\tfrac{1}{32}\pi-\tfrac{1}{4}+0.016)\ , \tag{B24}$$

which may be rewritten, using (B22) and $K_3=(2\pi^2)^{-1}$, as

$$\lambda=\lambda_\infty\left[1+\frac{\tilde{f}_\infty\pi}{8\kappa}[1-a_2\kappa^{-1}+O(\kappa^{-2})]\right]\ , \tag{B25}$$

with

$$a_2=\tfrac{16}{15}(\tfrac{1}{4}-\tfrac{1}{32}\pi-0.016)\frac{\tilde{f}_\infty}{w_\infty\chi}\ . \tag{B26}$$

The term of order κ^{-1} agrees precisely with our result (3.44) for both model E_0 and F. For model E_0 we have $\chi=1$, and in the case studied in Fig. 9, Eq. (8.26) yields $a_2=5.88\times 10^{-3}$, corresponding to the dot-dash curve, which is presumably exact as $\kappa^{-1}\to 0$. In the case of model F, a_2 is decreased by χ^{-1}, but remains positive, so that $\tilde{\lambda}_2$ remains negative. There is no reason to believe the calculation of Ref. 55 for model F, however, since v has not been treated consistently.

APPENDIX C: HIGH-TEMPERATURE REGIME: ANALYSIS OF DATA

We consider a high-temperature theory in the region $t\gtrsim t_m$ and a critical theory for $t\lesssim t_m$ with a matching point t_m at which both theories are supposed to be valid. The behavior in the high-temperature region is strongly influenced by the regular transients which appear in the bare theory, whereas these transients are neglected in the interior (critical) region. For $t\gtrsim t_m$ we have

$$\lambda(T,\kappa)=\lambda_\infty(T)\left[1+\frac{a_1\tilde{f}_\infty(T)}{\kappa^{1+\eta^A}}[1+\tilde{\lambda}_2(\kappa)]\right]\ , \tag{C1}$$

where according to Eqs. (B20), (3.21), and (3.27b)

$$a_1=[2(1+\eta^A)]^{-1}-\tfrac{1}{2}+\tfrac{1}{8}\pi=0.386\ , \tag{C2}$$

and the small correction $\tilde{\lambda}_2(\kappa)$ is assumed to be independent of regular transients. (In fact, we shall neglect $\tilde{\lambda}_2$ completely in the high-temperature region, but in a more accurate analysis it could be included in a self-consistent way.) We now set

$$\lambda_\infty(T)=\lambda_{\infty 0}+\lambda_{\infty 1}t+\lambda_{\infty 2}t^2+\cdots\ , \tag{C3}$$

$$\tilde{f}_\infty(T)=\tilde{f}_{\infty 0}+\tilde{f}_{\infty 1}t+\cdots\ , \tag{C4}$$

and fit the data for λ in the range $t_m<t<1$ to (C1)–(C4) with $\tilde{\lambda}_2=0$, treating the coefficients $\lambda_{\infty n}$ and $\tilde{f}_{\infty n}$ in (C3) and (C4) as adjustable parameters. The results of the fit are shown in Table VIII, for different values of t_m and with different numbers of coefficients retained. Fits 1 and 2 of Table VIII show that $\lambda_{\infty 2}$ is necessary for a good fit, whereas we conclude from fit 5 in Table VIII that $f_{\infty 1}$ should be discarded, even though its inclusion improves the fit. This is because $f_{\infty 1}$ turns out to be much larger than $f_{\infty 0}$ and its inclusion changes the other parameters substantially. We shall therefore retain fit 4 in Table VIII, with

$$t_m=10^{-2}\ , \tag{C5}$$

$$\lambda_\infty=\lambda_{\infty 0}=(1267\pm 12)\ \text{erg/sec cm K} \tag{C6}$$

$$\tilde{f}_\infty=\tilde{f}_{\infty 0}=(2.08\pm 0.16)\times 10^{-2}\ . \tag{C7}$$

These parameters will now be taken as the high-

temperature limit of the critical theory which describes the data in the interior region $t \lesssim t_m$. Specifically, we set $\lambda_\infty \approx \lambda_{01}$ and $\tilde{f}_\infty \approx \tilde{f}_{01} = f_{01}$, which yield [see Eqs. (B7), (B13), (B14), (C6), and (C7)]

$$w'_{01} = \lambda_0^2/2\pi^2\lambda_{01}^2 f_{01} = 0.48 \pm 0.04 \ . \tag{C8}$$

The initial value w''_{01} is not known, but we will pick various values and study the sensitivity of $\lambda(t)$ to this parameter. Choosing $w''_{01} = 0$, we may integrate the model F equations starting at $t = 1$ with (C7) and (C8) as the other initial conditions, and $B_3 = 0$. The ensuing $\lambda(t)$ is shown as the dot-dashed line for $t > t_m$ and the solid line for $t < t_m$ in Fig. 21. If we pick $w''_{01} = 0.3$ the curve for $\lambda(t)$ is shifted downward slightly so that it deviates from the data at $t = 10^{-3}$ but then crosses again near $t = 10^{-4}$; for $w''_{01} = -0.3$ the curve is shifted upward slightly and deviates from the data somewhat earlier than in Fig. 21. The accuracy of our initial values may be appreciated by comparing to the values

$$w'_{01} = 0.492; \quad f_{01} = 0.0194 \ , \tag{C9}$$

obtained by integrating fit 3 in part b of Table VI to $t = 1$ (these numbers result from a fit to the data in the range $10^{-6} < t < 10^{-2}$ with four adjustable parameters.) It is seen that (C7)–(C9) agree within the standard deviation of the high-temperature fit. In fact the value of $\lambda_\infty = \lambda_{01}$ extracted from (C9) agrees with (C6) within 2%. This means that if we use w'_{01} and f_{01} as given by (C7) and (C8) and adjust w''_{01} and B_3, we will obtain an excellent fit to the data in the whole range $10^{-6} < t < 10^{-2}$ (dashed line in Fig. 21, and fit 10 in part b of Table VI).

The above procedure could be improved by including the correction $\tilde{\lambda}_2$ in (C1) in a self-consistent way, and adjusting the functions $\lambda_\infty(T)$ and $\tilde{f}_\infty(T)$ with the following requirements: (i) Equation (C1) should fit experiment in the range $t > t_m$. (ii) At $t = t_m$, the thermal conductivity should satisfy

$$\lambda(T, \kappa) = \lambda(T_\lambda, \kappa) \ , \tag{C10}$$

i.e., regular transients should be negligible. Then the prediction for $t < t_m$ is obtained from model F with $\tilde{f}_\infty = f_{\infty 0}$ and $\lambda_\infty = \lambda_{\infty 0}$, which fixes w'_∞. The value of w''_∞ is not determined in the above procedure, so it must be picked arbitrarily (or from some other argument) and the sensitivity of the results to the choice of w''_∞ tested numerically.

[1]R. A. Ferrell, N. Menyhard, H. Schmidt, F. Schwabl, and P. Szepfalusy, Phys. Rev. Lett. 18, 891 (1967).

[2](a) G. Ahlers, Phys. Rev. Lett. 21, 1159 (1968); (b) also in *Proceedings of the Eleventh International Conference on Low Temperature Physics,* edited by J. F. Allen, D. M. Finlayson, and D. M. McCall (University of St. Andrews, St. Andrews, Scotland, 1968), p. 203.

[3]See also G. Ahlers, Rev. Mod. Phys. 52, 489 (1980).

[4]G. Ahlers, in *Proceedings of the Twelfth International Conference on Low Temperature Physics,* edited by E. Kanda (Academic, Japan, 1971), p. 21.

[5]M. Archibald, J. M. Mochel, and L. Weaver, in Ref. 2(b), p. 211.

[6]M. Archibald, J. M. Mochel, and L. Weaver, Phys. Rev. Lett. 21, 1156 (1968).

[7]L. E. Weaver, Ph.D. thesis (University of Illinois at Urbana, 1970) (unpublished).

[8]B. I. Halperin and P. C. Hohenberg, Phys. Rev. Lett. 19, 700 (1967); Phys. Rev. 177, 952 (1969).

[9]R. A. Ferrell, N. Menyhard, H. Schmidt, F. Schwabl, and P. Szepfalusy, Ann. Phys. (N.Y.) 47, 565 (1968).

[10]B. I. Halperin, P. C. Hohenberg, and E. D. Siggia, Phys. Rev. Lett. 32, 1289 (1974).

[11]B. I. Halperin, P. C. Hohenberg, and E. D. Siggia, Phys. Rev. B 13, 1299 (1976); 21, 2044(E) (1980).

[12]P. C. Hohenberg and B. I. Halperin, Rev. Mod. Phys. 49, 435 (1977).

[13]C. DeDominicis and L. Peliti, Phys. Rev. Lett. 38, 505 (1977); Phys. Rev. B 18, 353 (1978).

[14]V. Dohm and R. A. Ferrell, Phys. Lett. A 67, 387 (1978).

[15]V. Dohm, Z. Phys. B 31, 327 (1978).

[16]R. A. Ferrell and J. K. Bhattacharjee, J. Low Temp. Phys. 36, 165 (1979).

[17]V. Dohm, Z. Phys. B 33, 79 (1979).

[18]P. C. Hohenberg, B. I. Halperin, and D. R. Nelson, Phys. Rev. B 22, 2373 (1980).

[19]R. A. Ferrell and J. K. Bhattacharjee, Phys. Rev. Lett. 42, 1638 (1979).

[20]R. A. Ferrell and J. K. Bhattacharjee, in *Proceedings of the International Conference on Dynamic Critical Phenomena,* edited by C. P. Enz (Springer, New York, 1979).

[21]R. A. Ferrell and J. K. Bhattacharjee, in *Proceedings of the Second US-USSR Symposium on the Scattering of Light Condensed Matter,* edited by H. Z. Cummins (Plenum, New York, 1979).

[22]See Sec. III B and Appendix B of Ref. 18.

[23]A short version of the present paper appeared in G. Ahlers, P. C. Hohenberg, and A. Kornblit, Phys. Rev. Lett. 46, 493, 686(E) (1981). The fits described in this Letter were unfortunately based on incorrect weights assigned to the experimental points. The corrected analysis appears in the present paper, in particular in Figs. 16 and 17 which correspond to Figs. 1 and 2(a) of the Letter. As mentioned earlier [Phys. Rev. Lett. 47, 1419 (1981)], the main conclusions of the Letter are unaffected by the corrections.

[24]V. Dohm and R. Folk, Phys. Rev. Lett. 46, 349 (1981).

[25]V. Dohm and R. Folk, Z. Phys. B 40, 79 (1980).

[26]G. Ahlers and R. P. Behringer (unpublished).

[27]We are using the term "crossover" in its original sense

[see e.g., M. E. Fisher, Rev. Mod. Phys. 46, 597 (1974), Sec. VIII] of a change from one type of *critical* behavior to another, which can only occur if the crossover temperature t_c is itself much less than unity. Dohm and Folk use the term in a looser sense to mean the (nonlinear) evolution from a noncritical background to the asymptotic critical behavior. We are indebted to M. E. Fisher for an instructive conversation on this point.

[28]V. Dohm and R. Folk, Z. Phys. B41, 251 (1981).

[29]G. Ahlers, Phys. Rev. Lett. 43, 1417 (1979).

[30](a) T. J. Greytak, in Ref. 20; (b) J. A. Tarvin, F. Vidal, and T. J. Greytak, Phys. Rev. B 15, 4193 (1977); (c) W. F. Vinen and D. L. Hurd, Adv. Phys. 27, 533 (1978).

[31]B. J. Robinson and M. J. Crooks, Physica 107B, 339 (1981); and (unpublished).

[32]R. A. Ferrell and J. K. Bhattacharjee Phys. Rev. B 24, 5071 (1981).

[33]J. Kerrisk and W. E. Keller, Bull. Am. Phys. Soc. 12, 550 (1967); Phys. Rev. 177, 341 (1969).

[34]A. Onuki, Prog. Theor. Phys. (Kyoto) 64, 1902 (1980).

[35]G. Ahlers, J. Low Temp. Phys. 31, 429 (1978).

[36]D. S. Greywall and G. Ahlers, Phys. Rev. A 7, 2145(1973).

[37]R. P. Behringer and G. Ahlers (unpublished).

[38]See AIP document No. PAPS PRBMD-25-3136-16 of tabulated data. Order by PAPS number and journal reference from American Institute of Physics, Physics Auxiliary Publication Service, 335 East 45th Street, New York, N.Y. 10017. The price is $1.50 for each microfiche (98 pages), for $5 for photocopies of up to 30 pages with $0.15 for each additional page over 30 pages. Airmail additional. Make checks payable to the American Institute of Physics. This material also appears in *Current Physics Microfilm,* the monthly microfilm edition of the complete set of journals published by AIP, on the frames immediately following this journal.

[39]The specific heat is in units of inverse volume and g_b is a frequency; so λ in (2.1) has units of (length $\times$ time)$^{-1}$. It is customary to quote λ in erg/sec cm K, which corresponds to $\bar{\lambda}=\lambda k_B$. We shall suppress the bar, and use the same symbol for λ and $\bar{\lambda}$.

[40]P. C. Hohenberg, A. Aharony, B. I. Halperin, and E. D. Siggia, Phys. Rev. B 13, 2986 (1976).

[41]The value $\nu=0.675$ was derived from the superfluid density data of Ref. 36 by K. H. Mueller, G. Ahlers, and F. Pobell [Phys. Rev. B 14, 2096 (1976)], on the basis of a fit to a function which included a confluent singularity in addition to the leading power law. The amplitudes were treated as constants in this analysis. In very recent work, a regular temperature dependence for the leading amplitude was included, which reduced the exponent ν to 0.672 [G. Ahlers, in *Proceedings of the 1980 Cargese Summer Institute on Phase Transitions,* edited by M. Lévy, J. C. LeGuillou, and J. Zinn-Justin (Plenum, New York, 1981)]. Our use of the slightly larger value of ν is consistent with our neglect of all transients in κ.

[42]G. Ahlers, in *The Physics of Liquid and Solid Helium,* edited by K. H. Bennemann and J. B. Ketterson (Wiley, New York, 1976), Vol. I, Chap. II.

[43]G. Ahlers, Phys. Rev. A 8, 530 (1973).

[44]K. H. Mueller, G. Ahlers, and F. Pobell, Phys. Rev. B 14, 2096 (1976).

[45]H. A. Kierstead, Phys. Rev. 162, 153 (1967).

[46]J. F. Kerrisk, Ph.D. thesis (The University of New Mexico, 1968) (unpublished).

[47]R. W. Hill and O. V. Lounasmaa, Philos. Mag. 2, 143 (1957).

[48]G. Ahlers (unpublished).

[49]We use the subscript b to denote bare (i.e., unrenormalized) quantities, reserving the subscript zero for initial values of the renormalized parameters.

[50]K. G. Wilson and J. Kogut, Phys. Rep. 12, 75 (1974).

[51]Note that in Ref. 18 $\Lambda(l)$ should be replaced by $\Gamma(l)$ on the right-hand side (rhs) of Eq. (2.12), and the term f^2L should only appear once on the rhs of (B11). Furthermore, Eqs. (2.11) and (2.12) differ slightly from Eqs. (3.3) and (3.2) of the present paper, due to the presence of the static exponent η in the former work. The difference is associated with small differences in the renormalization procedure, but for consistency with Ref. 13 the definition should be as in the present paper.

[52]P. C. Hohenberg and S. Sarkar, Phys. Rev. B 24, 3800 (1981).

[53]E. Brézin, J. C. LeGuillou, and J. Zinn-Justin, in *Phase Transitions and Critical Phenomena,* edited by C. Domb and M. S. Green (Academic, New York, 1976), Vol. VI, p. 127.

[54]The coupling constant v is small everywhere so perturbation theory in v should be valid at all temperatures.

[55]J. K. Bhattacharjee and R. A. Ferrell (unpublished).

[56]In model E_0 the expansion is strictly in powers of κ_c/κ, whereas in model F this is only true for the first term, due to the presence of v which varies on the scale κ^{-1} and affects the function $\tilde{\lambda}_2(\kappa)$ in (3.46) (see Appendix B).

[57]L. G. Aslamazov and A. I. Larkin, Fiz. Tverd. Tela (Leningrad) 10, 1104 (1968) [Sov. Phys. Solid State 10, 875 (1968)]; Phys. Lett. 26A, 238 (1968).

[58]Other starting values in the range $-0.5 < w_{01}'' < 0.5$ do not alter the results appreciably.

[59]We have not quoted error bars for the parameters, but unless otherwise noted the *statistical* errors vary between ± 0.005 and ± 0.02 for f_0, w_0', w_0'', and B_3. In the tables we quote the numbers with three digits in order to facilitate reproducing the functions $w(l)$ and $f(l)$ numerically. No attempt has been made to estimate the *systematic* errors.

[60]See Ref. 23 and erratum, Phys. Rev. Lett. 46, 686 (1981).

[61]In actual fact B_3 should depend on w so there will be a variation with pressure of the three-loop contribution, since $w(l)$ depends on pressure via w_0. We neglect this variation.

[62]See the AIP document listed in Ref. 38.

[63]Note that since these represent analytic terms they will in principle apply below T_λ also.

[64]Equation (11) of Ref. 24 differs from Eq. (19) of Ref. 28 by the term $\frac{1}{8}f$ mentioned in Ref. 28 after Eq. (A8).

[65]W. B. Hanson and J. R. Pellam, Phys. Rev. 95, 321 (1954).

[66]The frequency $ak^{3/2}$ in Ref. 19 is actually $[\omega_m(k)\omega_\psi(k)]^{1/2}$; so it should be compared to $(B_sB_\psi)^{1/2}k^2$. In writing (5.2a) Ferrell and Bhattacharjee tacitly assume $w_b=B_\psi/B_s=1$.

[67]R. A. Ferrell, V. Dohm, and J. K. Bhattacharjee, Phys. Rev. Lett. 41, 1818 (1978).

[68]Our values for λ_∞ and λ_1 in Table II ($\lambda_\infty=1441$ erg/sec cm K, $\lambda_1=10^{-2}$ at vapor pressure and $\lambda_\infty=1445$ erg/sec cm K, $\lambda_1=3.3\times10^{-3}$ at $P=22.3$ bars) differ from those obtained by Ferrell and Bhattacharjee from the same data ($\lambda_\infty=1530$ erg/sec cm K, $\lambda_1=1.4\times10^{-2}$ at va-

por pressure, Ref. 32, and $\lambda_\infty = 1200$ erg/sec cm K, $\lambda_1 = 5 \times 10^{-3}$ at $P = 22.3$ bars, Ref. 20). The difference presumably arises because these authors did not have available data in numerical form.

[69]The case $f_{01} = 0.5$ shown in Fig. 10 has a small w^* and a large w_{01} and it clearly is well represented by the quadratic approximation displayed in Fig. 2 or 7 of Ref. 25 [because of the different initial conditions one must compare Fig. 10 above for $t < 1$ with the corresponding figures of Ref. 25 for $t < 10^{-3}$ ($l < 10^{-2}$)].

[70]In order to test the consistency between our numerical procedures and those of Ref. 25 we have also carried out a fit with adjustable ϵ in (3.16), but $\epsilon = 1$ in (3.13). The results (fit 1 in Table VII) with $t_0 = 10^{-3}$, are $w_0 = 0.482$, $f_0 = 0.844$, and $\epsilon = 1.02$ leading to $d - d^* \approx 0$, in good agreement with the corresponding values of Dohm and Folk, $w_0 = 0.45$, $f_0 = 0.87$, $d - d^* = -0.04$. When we fix ϵ at 1.06 (i.e., $d - d^* = -0.04$) we find (fit 7 in Table VII) $w_0 = 0.465$ and $f_0 = 0.856$.

[71]Note that contrary to what is implied by Dohm and Folk (Refs. 25 and 28) it is not the existence of new experimental data (cell A) which invalidates their result. Our criticisms and conclusions apply to the data they analyze (cell D) as well.

[72]V. Dohm and R. Folk, paper presented at the 16th International Conference on Low Temperature Physics, August 1981, Physica B (in press).